Interplay between wetting and phase separation in binary fluid mixtures: roles of hydrodynamics

2001 J. Phys.: Condens. Matter 13 4637

(http://iopscience.iop.org/0953-8984/13/21/303)

INSTITUTE OF PHYSICS PUBLISHING JOURNAL OF PHYSICS: CONDENSED MATTER

J. Phys.: Condens. Matter **13** (2001) 4637–4674 www.iop.org/Journals/cm PII: S0953-8984(01)20973-4

Interplay between wetting and phase separation in binary fluid mixtures: roles of hydrodynamics

Hajime Tanaka

Institute of Industrial Science, University of Tokyo, Meguro-ku, Tokyo 153-8505, Japan

Received 16 January 2001

Abstract

Here we consider how phase-separation kinetics and morphology are affected by the preferential wetting of a solid surface by one component of a binary fluid mixture. The behaviour is crucially dependent upon whether the spinodal decomposition is bicontinuous-type or droplet-type, i.e. the composition symmetry. Near a symmetric composition, wetting effects are strongly delocalized by hydrodynamic effects unique to bicontinuous phase separation. We discuss the physical mechanism of the unusually fast lateral growth of wetting domains found by Wiltzius and Cumming, the thickening dynamics of wetting layers, and pattern evolution under the influence of surface fields, focusing on the roles of hydrodynamics. We point out a novel possibility of double phase separation: that the quick hydrodynamic reduction of the interface area may spontaneously destabilize the phase-separated macroscopic domains and induce secondary phase separation. We also consider effects of the preferential wetting of immobile and mobile particles by one component of a fluid mixture on phase separation and the resulting complex pattern evolution. It is demonstrated that hydrodynamics always plays crucial roles in the pattern evolution of a phase-separating fluid mixture interacting with solid surfaces.

1. Introduction

Phase-separation phenomena have been extensively studied in the past three decades from both the experimental and the theoretical viewpoints [1, 2]. Since the finding of a complete–partial wetting transition near a critical point of a binary mixture by Cahn [3], wetting phenomena have also been intensively studied [4, 5]. In general, phase separation can never be free from surface effects since material should be confined in a container in any experiment. Thus, it is of fundamental importance to study how the preferential wetting of the surface by one component of a mixture affects the phase-separation kinetics and morphology evolution (see references [6–8] for review). For example, we are interested in the following questions:

(i) How far from the solid surface do wetting effects affect phase separation? What physical factors determine the degree of delocalization of the surface effects?
(ii) How do droplets 'feel' a solid wall?

0953-8984/01/214637+38$30.00

(iii) How is material transported toward the solid wall and how is the wetting layer formed?
(iv) What is the role of hydrodynamics?
(v) How does the geometry of confinement affect the final morphology?

In addition to these fundamental areas of interest, the understanding of wetting effects on phase separation and the resulting self-organization is also of practical importance in material processing, including the morphological control of nanomaterial, composite material and thin-film coating, which may become key technologies in the 21st century.

Phase separation produces two semi-macroscopic phases having different abilities to wet the surface of the third material, reflecting the difference in energy of interaction with the surface between the two phases. Thus the phases are spatially rearranged during phase separation to lower the total energy, including that of the solid–liquid interactions. The late stage of pattern evolution is governed by the complex interplay between the liquid–liquid and solid–liquid interfacial energies and the resulting hydrodynamic transport of material.

Here we discuss the wetting dynamics of a mixture undergoing phase separation in confined geometry, such as a quasi-one-dimensional (1D) or a quasi-two-dimensional (2D) capillary. *Throughout this article, a 1D capillary means a capillary tube, while a 2D capillary means a cell made of two parallel glass plates with a narrow gap.* We also discuss the effects of hydrodynamics on the pattern evolution, focusing on the composition symmetry. A container can in principle be gas, immiscible liquid, or solid. Since solid containers are most often used and practically most important, we here consider phase separation of fluid mixtures in contact with solid surfaces. A solid container imposes fixed-solid boundary conditions. The problems of effects of the moving boundary with gas and liquid on phase separation are beyond the scope of this article, although they are of practical importance in thin-film technologies (see, e.g., references [9,10] and references therein). We also consider how wetting mobile and immobile particles affects phase separation of a fluid mixture containing such particles.

The structure of this article is as follows. In section 2, we describe the theoretical background required to understand the phase-separation behaviour of fluid mixtures and the roles of hydrodynamics. In section 3, we show the results of experimental observation of pattern evolution in a confined geometry. In section 4, we discuss the early-stage wetting dynamics, focusing on the hydrodynamic effects, using a simple scaling argument. In section 5, we discuss the late-stage domain growth in a 2D capillary. In section 6, we describe the phenomenon of wetting-induced double phase separation and discuss its possible mechanism. In section 7, we discuss the effects of wetting immobile and mobile particles on phase separation. In section 8, we review the 3D numerical simulation studies of wetting effects on phase separation of fluid mixtures and check the validity of our physical picture and scaling argument. In section 9, we summarize our article.

2. Theoretical background

2.1. Bulk phase separation without surface effects

Since we are interested in macroscopic pattern evolution, we use the coarse-grained picture to consider the problem. The basic Langevin equations describing the dynamics of a fluid model (model H in the Hohenberg–Halperin notation) are [1,2,11,12]

$$\frac{\partial}{\partial t}\phi = -\boldsymbol{\nabla}\cdot(\phi \boldsymbol{v}) + L_\xi \nabla^2 \frac{\delta}{\delta \phi}(\beta H) + \theta \tag{1}$$

$$\rho \frac{\partial}{\partial t}\boldsymbol{v} = \boldsymbol{F}_\phi - \boldsymbol{\nabla} p + \eta \nabla^2 \boldsymbol{v} + \boldsymbol{\iota} \tag{2}$$

where ϕ is the composition, $\boldsymbol{v}$ is the velocity, $\beta = 1/k_BT$ (k_B: Boltzmann's constant), L_ξ is the renormalized transport coefficient, ρ is the density, η is the viscosity, and θ and $\boldsymbol{\iota}$ are thermal noises. The pressure p is determined to satisfy the incompressibility condition $\boldsymbol{\nabla} \cdot \boldsymbol{v} = 0$. Here H is the Ginzburg–Landau-type Hamiltonian given by

$$\beta H = \int \mathrm{d}\boldsymbol{r} \left[-\frac{1}{2}\tau\phi^2 + \frac{1}{4}u\phi^4 + \frac{1}{2}C|\boldsymbol{\nabla}\phi|^2 \right]. \tag{3}$$

In equation (2), $\boldsymbol{F}_\phi$ is the thermodynamic force density acting on the fluid due to the fluctuations of the composition ϕ and $\boldsymbol{F}_\phi = -\phi\,\boldsymbol{\nabla}\mu = -\boldsymbol{\nabla}\pi + k_BTK\phi\,\boldsymbol{\nabla}\nabla^2\phi$ (π: osmotic pressure), where $\mu = \delta H/\delta\phi$ is the chemical potential.

Before discussing the hydrodynamic effects on the wetting dynamics, we need to understand their effects on bulk phase separation, which can be described by the above set of equations. After the formation of a sharp interface, the interface profile can be approximately described by the local equilibrium composition profile of an interface, $\phi_{\mathrm{int}} = \phi_e \tanh(\zeta/\sqrt{2}\xi)$, where ϕ_e ($=\sqrt{|\tau|/u}$) is the equilibrium composition and ξ is the correlation length ($\xi = \sqrt{C/|\tau|}$). ζ is the distance from the interface defined by $\zeta = \boldsymbol{n} \cdot (\boldsymbol{r} - \boldsymbol{r}_a)$, where $\boldsymbol{r}_a$ is a point on the interface and $\boldsymbol{n}$ is the unit normal vector of the interface at the point $\boldsymbol{r}_a$ toward the domain with a positive value of ϕ. Then, the thermodynamic force density due to the interface $\boldsymbol{F}_\phi^{\mathrm{int}}$ can be expressed by

$$\frac{\boldsymbol{F}_\phi^{\mathrm{int}}}{k_BT} = -C\,\nabla^2\phi\,\boldsymbol{\nabla}\phi = -C(\boldsymbol{\nabla}\cdot\boldsymbol{n})\left(\frac{\partial\phi_{\mathrm{int}}}{\partial\zeta}\right)^2\boldsymbol{n}. \tag{4}$$

Note that the conserved part of the force cannot produce any velocity fields for an incompressible fluid and should be balanced with the pressure p. Here $\boldsymbol{\nabla}\cdot\boldsymbol{n}$ is the curvature at $\boldsymbol{r}_a$ and $\boldsymbol{\nabla}\cdot\boldsymbol{n} = 1/R_1 + 1/R_2$, where $1/R_1$ and $1/R_2$ are the two principal curvatures of the interface. Thus, we obtain the following equation by putting equation (4) into equation (2) and using the relation $k_BTC(\partial\phi_{\mathrm{int}}/\partial\zeta)^2 \cong \sigma\delta(\zeta)$ where σ is the interface tension:

$$-\boldsymbol{\nabla}p' - \sigma\left(\frac{1}{R_1} + \frac{1}{R_2}\right)\delta(\zeta)\boldsymbol{n} + \eta\,\nabla^2\boldsymbol{v} + \boldsymbol{\iota} = 0. \tag{5}$$

It is convenient in some cases to scale length and time, respectively, by the correlation length of composition fluctuations ξ and its lifetime $\tau_\xi = \xi^2/D_\xi$, where D_ξ is the renormalized diffusion constant given by $D_\xi = \tau L_\xi$. Upon scaling length and time and neglecting noises, equation (2) becomes $\partial\boldsymbol{V}/\partial t = \Gamma\boldsymbol{F} - \boldsymbol{\nabla}P + \Xi\,\nabla^2\boldsymbol{V}$, where $\boldsymbol{F}$ and $\boldsymbol{V}$ are the scaled $\boldsymbol{F}_\phi$ and $\boldsymbol{v}$, respectively. Here

$$\Gamma = \frac{\tau\phi_e^2\tau_\xi^2}{\rho\beta\xi^2}$$

where $\pm\phi_e$ are final equilibrium compositions, and

$$P = \frac{\tau_\xi^2}{\rho\xi^2}p \qquad \Xi = \frac{\eta\tau_\xi}{\rho\xi^2}.$$

Then, the fluidity parameter R_f is defined as

$$R_f = \frac{\Gamma}{\Xi} = \frac{\tau\phi_e^2\tau_\xi}{\eta\beta} = 6\pi\tau\phi_e^2\xi^3 = 18\pi\sigma\xi^2\beta \tag{6}$$

where the relation $\sigma/k_BT = \frac{1}{3}\tau\xi\phi_e^2$ is used. This parameter R_f is a measure of the relative importance of the streaming term (hydrodynamics) versus the diffusion term (diffusion). It should be noted that for 3D, R_f is a universal constant near a critical point [2] and estimated as $R_f = 18\pi A_\sigma = 5$–10 since $\sigma = A_\sigma k_BT/\xi^2$, where A_σ is a universal constant and

$A_\sigma = 0.1$–0.2. Thus, the fluidity is not a control parameter in a critical regime. In the mean-field regime, however, this is not necessarily the case. This point will be discussed later in section 6.2.2.

On the basis of the above equations, we consider the domain coarsening kinetics in the late stage of phase separation. Under the incompressibility condition, *the domain geometry*, which we call the '$\boldsymbol{n}$-pattern', selects the coarsening mechanism. Thus we consider bicontinuous phase separation of symmetric fluid mixtures and droplet phase separation of off-symmetric fluid mixtures separately. In both cases, the most important concept as regards understanding the kinetics of *bulk phase separation* is the self-similar growth of domains, which ensures the existence of only one length scale, namely, the domain size R.

(A) *Bicontinuous phase separation of symmetric fluid mixtures.* For a symmetric composition ($\Phi_A \sim 1/2$; Φ_A: the volume fraction of the A-rich phase), the second term in the right-hand side of equation (5), which is the capillary pressure, produces the velocity fields of $v \sim \sigma/\eta$ that lead to the growth law $R \sim (\sigma/\eta)t$ (Siggia's mechanism [13]). The scaled version is $R/\xi = b_h(t/\tau_\xi)$, where b_h is a universal constant. Such a linear growth was confirmed experimentally [14–18]. Note that the non-divergent character of the $\boldsymbol{n}$-pattern of a bicontinuous structure allows the second term of equation (5) to directly produce the velocity fields even under the incompressibility condition. The flow in bicontinuous tubes is driven by the gradient in the capillary pressure and its mechanism is basically the same as the Rayleigh instability of a fluid tube.

(B) *Droplet phase separation of off-symmetric fluid mixtures.* For an off-symmetric composition ($\Phi_A \not\simeq 1/2$), on the other hand, the $\boldsymbol{n}$-pattern of droplet morphology has a divergent character. Thus, the second term in equation (5) has to be balanced with $\boldsymbol{\nabla} p$ to satisfy $\boldsymbol{\nabla} \cdot \boldsymbol{v} = 0$ and cannot produce any velocity fields except during collision. Accordingly, there is a pressure difference of $2\sigma/R$ across the interface (Laplace's law), while there are no macroscopic velocity fields ($\boldsymbol{v} = 0$), or no interparticle interactions. The latter fact is the basis of the Brownian-coagulation mechanism [13, 19], which assumes that there are no interparticle interactions and the droplet motion is driven purely by thermal force noises $\boldsymbol{\iota}$ in equation (2). In this case, the domain coarsening is driven by a process of hydrodynamic diffusion of droplets. By considering diffusion of a droplet of size R over the interdroplet distance $\sim R$, we straightforwardly obtain $R^2 \sim D_R t$, where $D_R \sim k_B T/(5\pi\eta R)$. This leads to the coarsening law $R \sim (k_B T/\eta)^{1/3} t^{1/3}$. The scaled version is $R/\xi = b_d(t/\tau_\xi)^{1/3}$, where b_d is a universal constant. This mechanism is well known as the Brownian-coagulation (Binder–Stauffer) mechanism [1, 2, 13]. It should be noted that there may exist some additional mechanisms of droplet coarsening in fluid mixtures [20–23], which originate from the coupling of composition (diffusion) and velocity fields (convection). This may play a role in the wetting kinetics of droplets in a fluid mixture, although we do not dwell on this problem in this article.

As will be shown later, these two coarsening mechanisms also play crucial roles in fluid phase separation under the surface fields, and the above scaling argument is quite useful for understanding the kinetics of wetting.

2.2. Phase separation under surface effects

In the coarse-grained picture, the surface contribution due to the existence of a wall at $z = 0$ can be included into the Hamiltonian as

$$\beta H_{\text{total}} = \int_{z \geqslant 0} \mathrm{d}\boldsymbol{r} \left[-\frac{1}{2}\tau\phi^2 + \frac{1}{4}u\phi^4 + \frac{1}{2}K|\boldsymbol{\nabla}\phi|^2 + f_s(\phi)\delta(z) \right] \tag{7}$$

where

$$f_s(\phi) = a\phi - (b/2)\phi^2$$

(a and b are constants depending upon the surface properties) [7,8]. Here the z-axis is chosen to be perpendicular to the solid surface. The kinetic equations (equations (1) and (2)) with this Hamiltonian should describe the phase-separation dynamics under the influence of surface fields. However, it is difficult to gain physical insight into the complex dynamics directly from these equations. There are two approaches to gaining a theoretical understanding of the kinetics of wetting during phase separation in fluid mixtures. One is a phenomenological approach, which is based on the scaling argument for the domain coarsening. The other is that of solving the above equations numerically. The results of these two approaches will be described later.

Before discussing the dynamics of pattern evolution, we first consider the equilibrium problem, since knowledge about the final structure to be formed is important for the understanding of pattern-evolution kinetics.

2.3. Composition symmetry and final equilibrium structures

Here we discuss how the composition symmetry affects the final equilibrium configuration in a confined geometry. In the following we assume that the wetting layer is thick enough to allow neglect of the disjointing pressure.

2.3.1. Confinement in a 2D capillary. In the late stage of phase separation, we need to consider only the free energy originating from the interface since the bulk part of the free energy is already minimized there. Thus, the energetic factors to be considered are the interface and the surface contact energy. There are two possible final configurations for a 2D capillary: (1) a layer structure (complete wetting configuration) and (2) a disc-like droplet structure (partial wetting configuration) (see figure 1). The free energies per unit area for the configurations of complete and partial wetting are given by

$$F_{cw} = 2(\gamma_\alpha + \sigma) \qquad F_{pw} = 2\phi_\alpha\gamma_\alpha + 2\phi_\beta\gamma_\beta + \sigma f(d)$$

respectively. σ is the interfacial tension between the α- and β-phases and γ_i is the interfacial tension between the i-phase and the wall. ϕ_α and ϕ_β are the volume fractions of the α- and β-phases, respectively. Here the α-phase is more able to wet the wall than the β-phase. $f(d)$ is the total area of the interface between the α- and β-phases per unit area. Neglecting the last term in F_{pw},

$$F_{cw} - F_{pw} = 2\sigma(1 - \phi_\beta\Delta\gamma/\sigma)$$

where $\Delta\gamma = \gamma_\beta - \gamma_\alpha$. The morphological transition occurs at $\phi_\beta = \sigma/\Delta\gamma$.

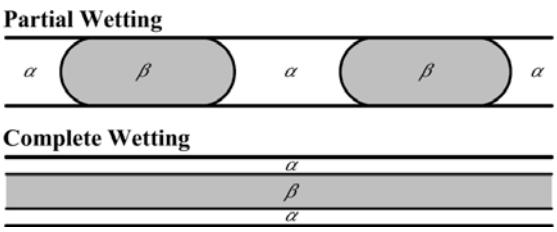

Figure 1. Final equilibrium structures for partial and complete wetting. Here the α-phase is more able to wet the solid wall than the β-phase.

2.3.2. Confinement in a 1D capillary. As discussed by Liu *et al* [24], the free energies per unit length for the configurations of complete and partial wetting (*tube* and *plug*) (see figure 1) for a 1D capillary are given by

$$F_{cw}/2\pi = r_c\sigma + r_0\gamma_\alpha \qquad F_{pw}/2\pi = r_0[\phi_\alpha\gamma_\alpha + \phi_\beta\gamma_\beta] + g(r_0)\sigma$$

respectively. Here r_c is the radius of the fluid *tube* for the complete wetting configuration and $r_c^2 = \phi_\beta r_0^2$. $g(r_0)$ is the total area of the interface between the α- and β-phases per unit length for the partial wetting configuration. Provided that the last term in F_{pw} is negligible,

$$(F_{cw} - F_{pw})/2\pi = r_0\sigma[\phi_\beta^{1/2} - (\Delta\gamma/\sigma)\phi_\beta].$$

The transition between the complete and partial wetting configurations occurs at $\phi_\beta = (\sigma/\Delta\gamma)^2$.

Since $\sigma = \sigma_0\epsilon^\mu$ ($\mu = 1.26$) and $\Delta\gamma = \Delta\gamma_0\epsilon^\delta$ ($\delta = 0.34$) where $\epsilon = (T - T_c)/T_c$, the transition composition is given by $\phi_t = (\sigma_0/\Delta\gamma_0)\epsilon^{(\mu-\delta)}$ for a 2D capillary and by $\phi_t = (\sigma_0/\Delta\gamma_0)^2\epsilon^{2(\mu-\delta)}$ for a 1D capillary. For both 1D and 2D capillaries, thus, the partial wetting configuration is energetically favoured near the symmetric composition for a deep quench.

It should be noted that the above lowest-energy configuration is not necessarily realized in a straightforward manner since there may be no direct kinetic path to it. Thus, the kinetic factors are quite important in the mechanism of pattern evolution. This point will be discussed later, focusing on the roles of hydrodynamics.

3. Pattern evolution in confined geometry: experimental observation

Hereafter we show the results of experimental observation, which tell us how a homogeneous mixture reaches the final phase-separated structure described above in a confined geometry. Although a number of pioneering works on the effects of wetting on morphological evolution in a fluid mixture [25–32] for various conditions have appeared, we here summarize our own studies on how wetting effects affect the pattern evolution of phase separation in fluid mixtures *on a macroscopic level*. We put a special focus on the roles of hydrodynamics.

3.1. Phase separation in a 1D capillary [33, 34]

First we consider wetting effects on phase separation in binary mixtures confined in a 1D capillary. This geometry is quite useful for getting information on the evolution of phase-separated structures along the surface normal, which is very difficult to obtain in usual experimental configurations. This is possible because we can see through to the inside of a capillary tube by optical microscopy. Figures 2(a)–2(c) show the pattern evolution during phase separation of poly(vinyl methyl ether) (PVME)/water mixtures confined in 1D capillaries. This mixture has a lower-critical-solution-temperature-type phase diagram and the water-rich phase is more able to wet (we term this being more 'wettable' subsequently) the glass wall than a PVME-rich one (see figure 1 of reference [33] for the phase diagram). Pattern evolution can be grouped into three types in terms of the composition symmetry; the symmetric critical composition is PVME/water (7/93) (weight ratio).

(a) **Case (a) (see figure 2(a)).** When a more wettable phase is a majority phase, non-wettable droplets coarsen with time mainly by the Brownian-coagulation mechanism. Note that a more wettable matrix phase naturally covers the solid wall from the beginning for this case. Droplets slowly move toward the symmetric axis of the capillary tube with coarsening. Eventually, non-wettable droplets of size comparable to that of the tube align on the axis.

The droplet size finally exceeds the pore size (the crossover from three dimensions (3D) to one dimension (1D)), and the droplets transform into capsules. Before the dimensional crossover, however, the coarsening becomes extremely slow for the following reasons: (1) the translational motion of droplets along the tube is strongly suppressed due to the narrow gap between a droplet and the tube, which slows down the rate of flow, and (2) the lack of difference in curvature between droplets makes the evaporation–condensation mechanism [1, 2] ineffective. Note that the curvature is determined solely by the tube diameter.

(b) **Case (b) (see figure 2(b)).** When the minority phase is more able to wet glass, the droplets gradually wet the glass and form a wetting layer. More precisely, droplets move toward the solid wall by diffusional motion, hit the wall, and eventually wet it. The resulting wetting layer is stable for a strongly asymmetric case, but it becomes unstable for a weakly asymmetric case and transforms into a bridge structure. Hydrodynamic stability analysis indicates that the layer or unduloid configuration is stable for a thinner film. It should be noted that the formation of the wetting layer is very much slower for this case than for symmetric mixtures, since the former is governed by droplet diffusion but the latter by direct hydrodynamic transport (see table 1 in reference [33]).

(c) **Case (c) (see figure 2(c)).** When the composition is nearly symmetric, bicontinuous phase separation proceeds in the initial stage. Then the macroscopic wetting layer is rapidly formed. It grows by the hydrodynamic pumping of fluid through the fluid tube connected to the wetting layer. After the formation of the complete wetting layer, the Rayleigh instability leads to the formation of bridges [33]. This instability is a result of the competition between the destabilizing effect of the transverse curvature at long wavelengths and the stabilizing effect of the longitudinal curvature at short wavelengths. This instability is characteristic of a 1D capillary. There is no analogous instability in a 2D capillary since the area of the planar interface is always increased by small perturbations to it. After the formation of a bamboo-like structure, there is almost no coarsening because the reasons for the slow coarsening for case (a) (see reasons (1) and (2)) apply in this case even more strictly. Thus, the characteristic length scale of the final structure is determined solely by the diameter of a capillary tube. Domains stop growing at a finite size due to the lack of a kinetic path. This behaviour is markedly different from that in the case of a 2D capillary, where domains keep growing without limit in lateral directions.

3.2. Phase separation in a 2D capillary [34, 35]

The basic features are the same as those of the above cases for a 1D capillary. The pattern evolution can also be classified into three types in terms of the composition symmetry, in the same manner as for phase separation in a 1D capillary.

(a) **Case (a) (see figure 3(a)).** When a less wettable phase is a minority phase, less wettable droplets coarsen with time mainly by the Brownian-coagulation mechanism and grow in size. Spherical droplets transform into disc-like ones when their diameter $2a$ exceeds the spacing d. After this transformation, the droplet radius a keeps growing as a result of direct collisions between droplets as $a \sim t^{1/3}$. Although this time exponent is consistent with the prediction of the Brownian-coagulation mechanism, there is an experimental indication that there is attractive interaction between droplets. We proposed [20, 21] that the coupling between concentration fields around droplets induces convective flow, which effectively causes attractive interaction and moves droplets hydrodynamically. There are some theoretical studies, which try to explain this behaviour along the above lines [22, 23].

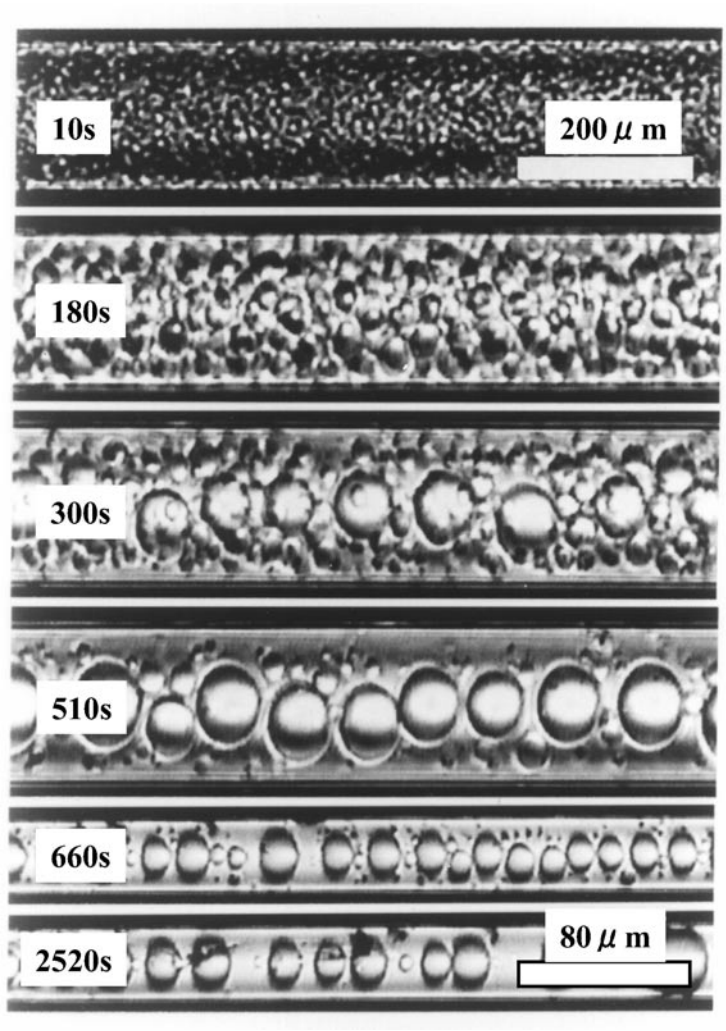

(a)

Figure 2. Pattern evolution during phase separation of a mixture of poly(vinyl methyl ether) (PVME) and water in a 1D capillary, whose walls are observed as thick black horizontal lines in the figures. (a) Pattern evolution in PVME/water (5/95) after a temperature jump from $T = 32.5\ ^{\circ}$C to $T = 33.9\ ^{\circ}$C. (b) Pattern evolution in PVME/water (10/90) after a temperature jump from $T = 32.5\ ^{\circ}$C to $T = 33.1\ ^{\circ}$C. (c) Pattern evolution in PVME/water (7/93), which is near the critical (or symmetric) composition, after a temperature jump from $T = 32.5\ ^{\circ}$C to $T = 33.4\ ^{\circ}$C. Note the large difference in coarsening rate between the droplet ((a) and (b)) and bicontinuous (c) cases.

Although there seem to be no apparent effects of wetting on this phenomenon, further studies are necessary to completely rule out such effects and clarify the relevant mechanism of droplet coarsening.

(b) **Case (b) (see figure 3(b)).** When a more wettable phase is a minority phase, droplet spinodal decomposition takes place initially. However, droplets move toward the walls and start to wet the glass surfaces. As a result, its number density keeps decreasing. The wetting speed is much slower than in bicontinuous phase separation as in the case of 1D

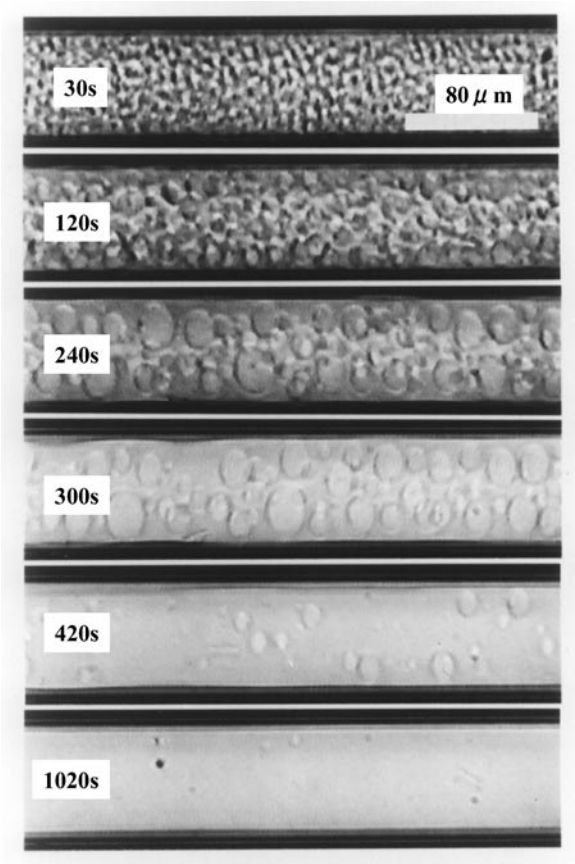

(b)

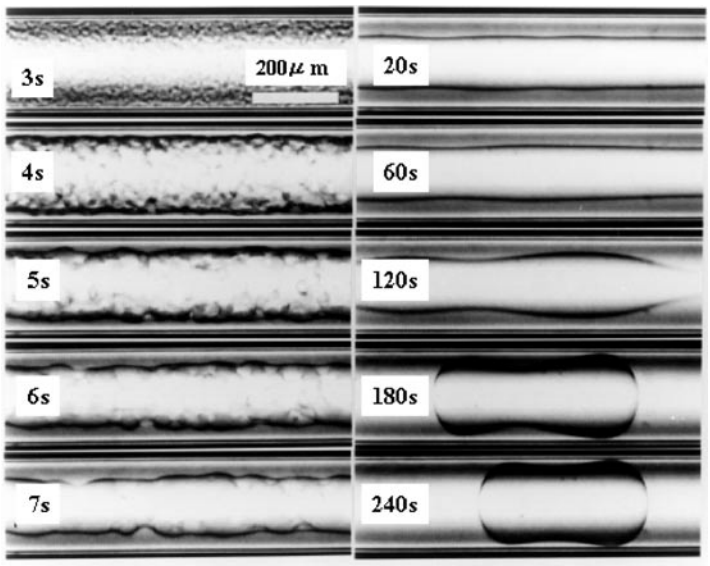

(c)

Figure 2. (Continued)

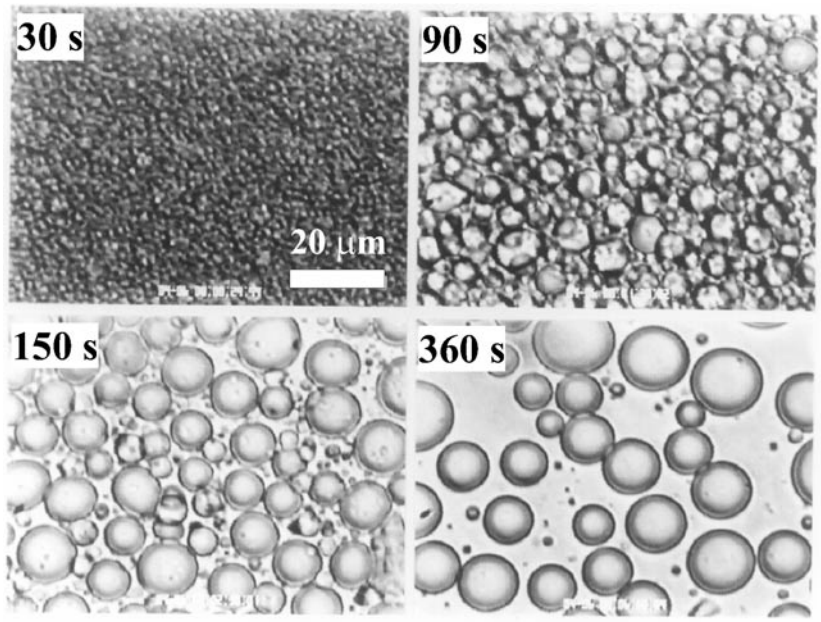

(a)

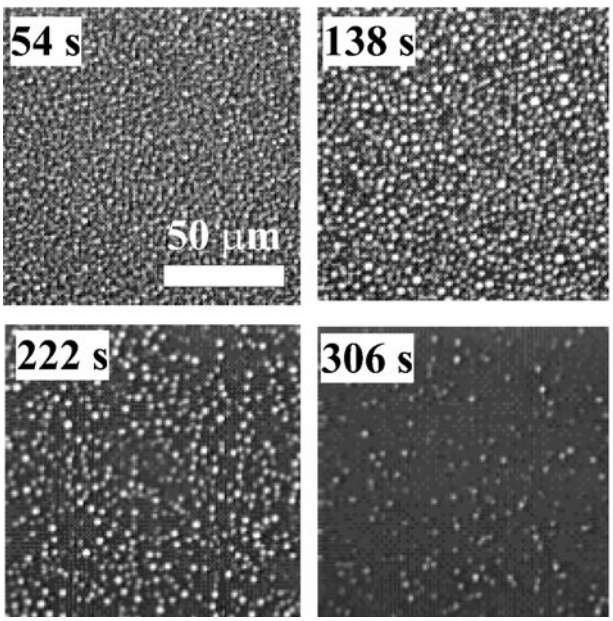

(b)

Figure 3. Pattern evolution during phase separation of fluid mixtures in a 2D capillary. (a) Pattern evolution in PVME/polystyrene (4/6) after a temperature jump from $T = 165\ ^{\circ}$C to $T = 180\ ^{\circ}$C. The gap was $d = 7.1\ \mu$m. (b) Pattern evolution in ϵ-caprolactone oligomer (OCL)/styrene oligomer (OS) (2/8) after a temperature jump from $T = 140.0\ ^{\circ}$C to $T = 110.0\ ^{\circ}$C. The gap was $d = 7.1\ \mu$m. (c) Pattern evolution in PVME/water (7/93), which is near the critical (or symmetric) composition, after a temperature jump from $T = 32.0\ ^{\circ}$C to $T = 33.3\ ^{\circ}$C. The gap was $d = 3\ \mu$m.

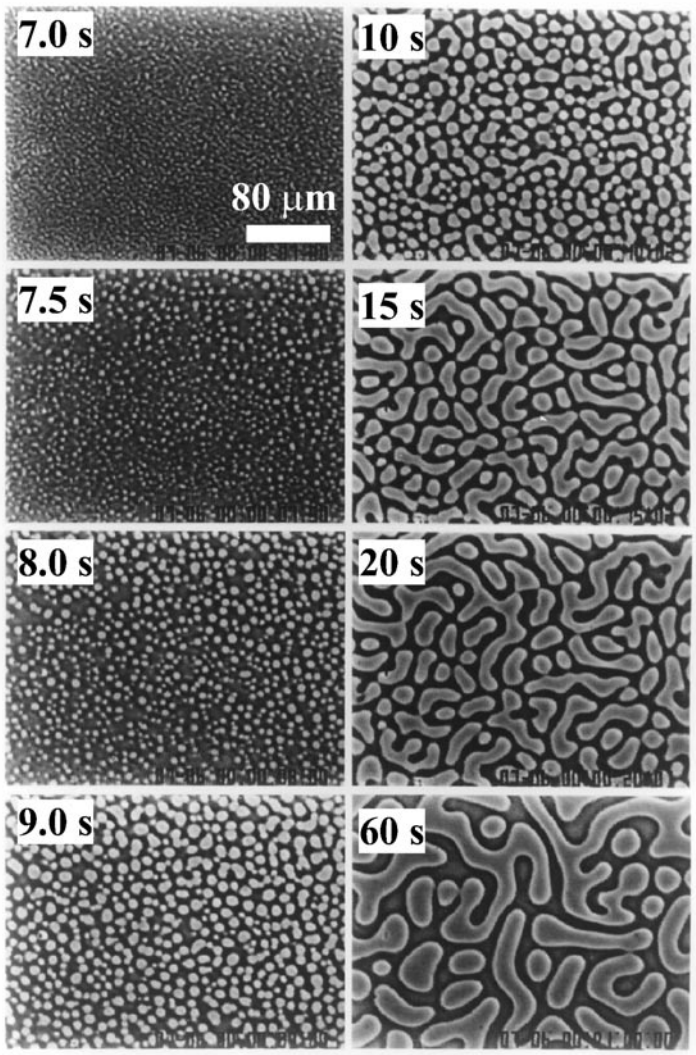

(c)

Figure 3. (Continued)

capillaries. This is because the hydrodynamic pumping mechanism, which is the cause of the fast coarsening for bicontinuous phase separation, does not operate for droplet phase separation. Eventually, all the droplets are absorbed in the wetting layers and thus become invisible. This process results in a three-layer sandwich structure (see figure 1(b)): two wetting layers of a more wettable phase and one sandwiched layer of a less wettable phase. This configuration is stable against fluctuations unless the gravitational effects destabilize it. The formation of complete wetting layers is supported by the fact that in optical microscopic observations all the droplets completely disappear after a long time. The details of the wetting kinetics will be discussed elsewhere [36].

(c) **Case (c) (see figure 3(c)).** When the composition is nearly symmetric, bicontinuous phase separation proceeds initially. One expects, from the case of a 1D capillary, the wetting

layer to be quickly formed by a hydrodynamic process. The interconnectivity of the bicontinuous structure allows the hydrodynamic pumping of fluid into the wetting layers. Thus, the more wettable phase is transported into the wetting layer in a very efficient manner. Tubes start to bridge the two wetting layers and form disc-like droplets from the tubes bridging the upper and lower plates. Here we call them droplets. As discussed later, only the droplets whose lateral size is larger than the gap can grow, while all the other small droplets just disappear. Then these larger droplets start to attract each other by wetting-induced attractive interaction, which is driven by the hydrodynamic capillary instability of the tube formed between the two droplets (see section 5.2). During this process, the more wettable phase in the wetting layer turns back into droplets bridging the two wetting layers since the pressure inside the droplets is lower than that in the wetting layer. Accordingly, the apparent droplet area increases with time and eventually the total area fraction of the more wettable droplets approaches 50%, which is the volume fraction of the more wettable phase. This leads to the in-plane morphological transformation from a droplet to an interconnected structure in the late stage. This apparent change in the phase symmetry in an x–y plane can be explained by the existence of the wetting layer composed of the more wettable phase, which is hidden in the observation geometry, and its thinning.

Here we learn that the basic phase-separation behaviour in a 2D capillary is the same as that in a 1D capillary. The only difference comes from the stability of the interface of the wetting layer, which crucially depends on the dimensionality of the confinement geometry.

4. Early-stage wetting dynamics characteristic of bicontinuous patterns: scaling argument

Here we consider how the phase-separation pattern transforms from the initial bicontinuous pattern free from wall effects to a configuration strongly influenced by the preferential wetting of the walls by one component of a mixture. For bicontinuous phase separation, the hydrodynamics due to the capillary instability [33, 34, 37] plays a crucial role in the coarsening under the influence of wetting. Near the symmetric composition, the wettability is important mainly in the very initial stage to establish the initial configuration where the surface is covered by the wetting layer, to which the bicontinuous tubes are connected. This initial configuration establishes the anisotropic pressure gradient from the bicontinuous tubes in the bulk to the wetting layer. Thus, the more wettable phase can be continuously supplied into the wetting layer through the percolation tubes until the tube network disappears. Because of the percolation structure of a bicontinuous pattern in bulk, the wetting effect is not localized near the wall and strongly affects the whole sample. Thus, phase separation can be seriously affected by wetting phenomena especially near the symmetric composition even though a sample size is macroscopic. This means that we need to exercise special care if we intend to study bulk phase separation free from surface effects.

4.1. Dynamics of lateral growth of wetting domains: fast-mode kinetics

Here we discuss the initial stage of the wetting droplet formation [38, 39]. This problem was experimentally studied for a 2D capillary by Wiltzius and Cumming [29]. They found that the size of the wetting droplet l grows as $t^{3/2}$. This is the fastest coarsening ever found for phase separation and thus the phenomena have attracted considerable attention. Nevertheless, the physical origin of this unusually fast growth of domains is still not clear even now, although some mechanisms have been proposed and discussed [34, 37, 40–42].

Hereafter we propose a possible scenario [34,42], although its validity is yet to be checked carefully. We believe that this fast-mode kinetics is of purely hydrodynamic origin. This is our basic standpoint. There is a pressure gradient between a bicontinuous tube and its wetting part, reflecting the difference in transverse curvature of the tube between them. Thus there should be directional hydrodynamic flow from the tube to the wetting droplet. Since the pressure gradient between the tube and the wetting layer is $\sim\sigma/a$ over the distance a, the flux of this flow is estimated as $Q \sim (\sigma/\eta)a^2$, where η is the viscosity and a is the characteristic size of the tube.

Provided that the limiting factor as regards the droplet spreading is the supply of the more wettable phase from the tubes in the bulk by hydrodynamic flow, we get the relation $l\ \mathrm{d}l/\mathrm{d}t \sim Q$. Here we assume 2D growth of the wetting disc. This assumption may be valid for the case of *strong wettability* and it is supported by the 2D nature of the droplet growth confirmed experimentally [29,43]. Using Siggia's growth law for bulk, $a \propto (\sigma/\eta)t$, we obtain the relation $l \sim [(\sigma/\eta)t]^{3/2}$. This is consistent with observation. The prefactor $(\sigma/\eta)^{3/2}$ is roughly proportional to $(\Delta T)^{3\nu}$, where ΔT is the quench depth, ν is the critical exponent for the correlation length ξ, and $\nu \sim 0.63$. This dependence of the prefactor on ΔT is also found to be consistent with the experimental results [29,39,43].

For a weak-wetting case, the droplet spreading may not be purely two dimensional. For three-dimensional droplet growth, for instance, we obtain $l^2\ \mathrm{d}l/\mathrm{d}t \sim Q$. Thus we can generalize the relation $l \sim [(\sigma/\eta)t]^{3/D}$, where D is the spatial dimensionality of the wetting droplet. For hemispherical droplet growth ($D = 3$), $l \sim t$, while for disc-like droplet growth ($D = 2$), $l \sim t^{3/2}$ (see figure 4). The transitional behaviour for the exponent going from 1 to 3/2 observed by Cumming *et al* [44] may be explained by the above idea.

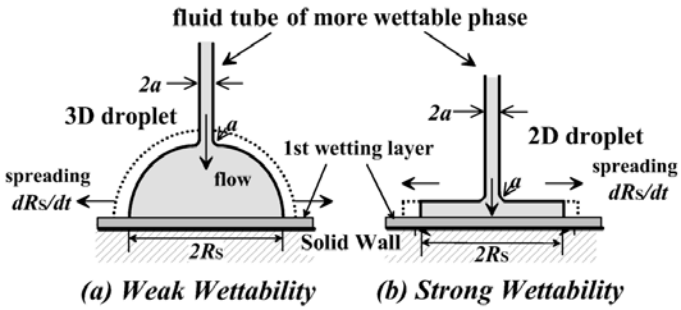

Figure 4. A schematic diagram of hydrodynamic coating, i.e. spreading droplets for $D = 3$ (a) and $D = 2$ (b). D is the dimensionality of the wetting droplet.

In a real situation, we also have to consider the coupling between tubes. Here we point out that a similar argument may be applied to the wetting tube instead of the wetting droplet, as schematically shown in figure 5. There should be growing and decaying tubes, which are connected to the wetting layers. If the tube thickens with time in the radial direction but does not grow along the tube axis direction, we again obtain $l \sim [(\sigma/\eta)t]^{3/2}$ from the same argument. If the tube grows three dimensionally in both directions, we obtain $l \sim (\sigma/\eta)t$. This scenario seems to more naturally explain the in-plane spatial correlation of wetting domains, which is responsible for the appearance of the scattering peak. Since in the above discussion there are some assumptions that cannot be justified in a convincing way, we need further studies to elucidate the relevant mechanism. For example, we do not have a convincing explanation for the 2D nature of coarsening. At this point, we have to say that this problem is still open.

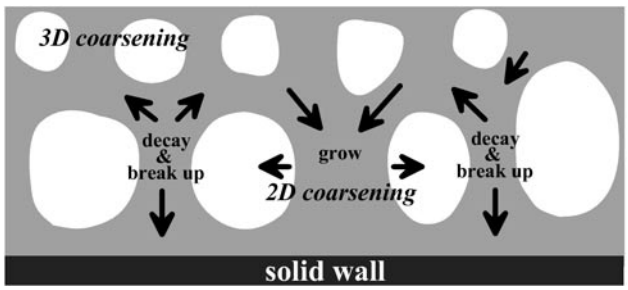

Figure 5. A schematic diagram of the growth kinetics near the wetting layer and a possible coupling between tubes.

4.2. Thickening dynamics of a wetting layer

Next we discuss the thickening dynamics of the wetting layer. It is known that the wetting layer grows as a logarithmic law [31, 45] or a power law with various exponents ranging from 0.1 to 1 [26, 34, 37, 45–49]. Here we focus on the late-stage thickening dynamics of the wetting layer in a fluid mixture [33, 34]. This mechanism should be common to all confined geometries as long as the inverse of the curvature of the solid surface is much larger than the radius of the tubes connected to the wetting layer. Once the wetting layer completely covers the whole surface and becomes homogeneous in a lateral direction, the rate of thickening of the wetting layer $(\mathrm{d}/\mathrm{d}t)d_w$ should be proportional to the flux from the bicontinuous tubes. The flux from a single tube Q can be estimated as $Q \sim (\sigma/\eta)a^2$. The number of tubes per area S is proportional to S/a^2. Thus the total flux Q_t is proportional to $S(\sigma/\eta)$. Since the thickening of the wetting layer is caused by this flux, $S\,(\mathrm{d}/\mathrm{d}t)d_w \sim S(\sigma/\eta)$. Therefore, we obtain the relation $d_w = k_w(\sigma/\eta)t$, where k_w is the proportionality constant. This linear growth behaviour is consistent with the observation in 1D capillaries, which is demonstrated in figure 6. The decrease in the slope with decreasing quench depth ΔT reflects the decrease in the interface tension σ with decrease in ΔT. Note that $\sigma \sim (\Delta T)^{2\nu}$. The linear growth of the wetting layer thickness was also confirmed by our numerical simulations [50], as will be shown in section 8.4.

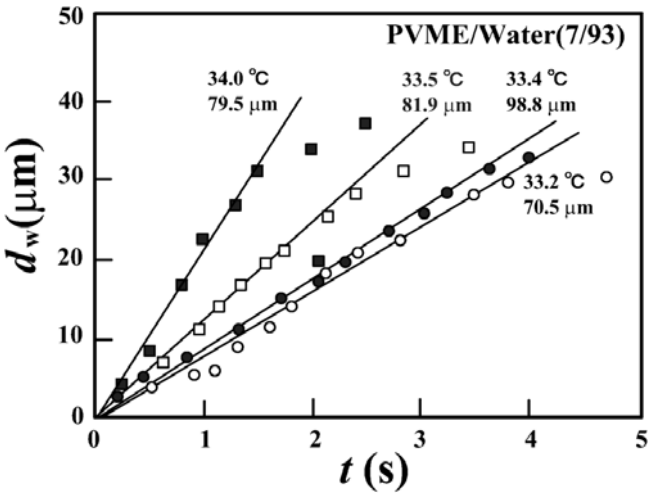

Figure 6. The temporal change in the wetting layer thickness measured in the 1D-capillary experiments.

4.3. The effect of the spatial dimensionality of confinement on wetting

Here we discuss the difference in the late stage of pattern evolution between 1D and 2D capillaries. For a 1D capillary, the tube radius of the bicontinuous pattern a can never exceed the capillary tube radius r_0, since the domain size cannot exceed r_0 in the radial direction because of the strong geometrical constraint. Thus the complete layer configuration is always formed first and then the Rayleigh instability leads to a stable bridge (or bamboo-like) structure [33]. In a 2D capillary, on the other hand, the tube diameter $2a$ can exceed the spacing d, since there is no geometrical restriction parallel to the plates. Once $2a$ becomes larger than d, the longitudinal curvature of the tube ($\sim 2/d$) becomes larger than its transverse curvature ($\sim 1/a$) [1]. Thus the pressure in the tube becomes lower than that in the wetting layer. Therefore, the tube bridging the two walls, whose radius a is larger than $d/2$, starts to thicken over time by absorbing the wetting layers. On the other hand, the tube bridging the two walls, whose radius a is smaller than $d/2$, is not formed or disappears. An example of such behaviour is shown in figure 7. The mechanism is schematically illustrated in figure 8(a). In accord with the above prediction, we found that a 2D disc-like droplet appearing in a 2D capillary, which can keep growing, always has an initial diameter $2a_0$ comparable to the thickness d [34], as indicated in figure 8(b). A similar observation was also made by Bodensohn and Goldburg [32]. The relation may be universal to all binary liquid mixtures and also to all quench conditions.

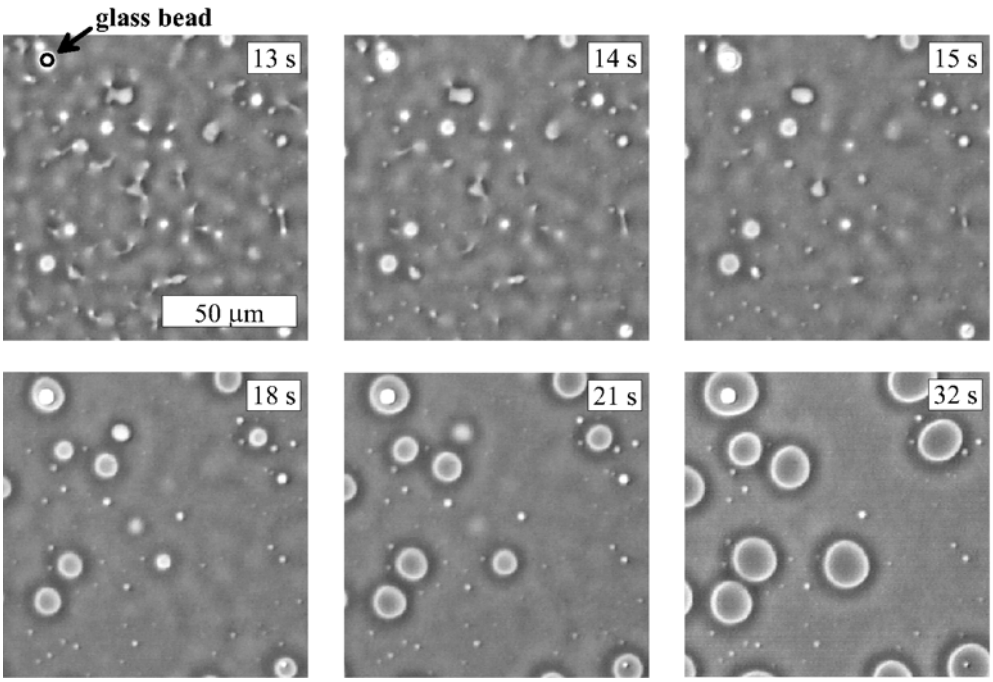

Figure 7. Pattern evolution during phase separation of a mixture of polystyrene (PS) ($M_w = 96\,000$) and diethyl malonate (DEM) confined in a 2D capillary. The composition was 10.7 wt% PS. The temperature was quenched from 3.7 °C to 3.2 °C. The critical temperature was 3.5 °C. The bright spot in the upper left corner is a glass bead used as a spacer, whose diameter is 4.9 μm. Its diameter is the same as the spacing d. Note that only the tubes bridging the two glass plates whose diameter is larger than the spacing can grow further in thickness.

[1] In this estimate of the longitudinal curvature of the tube, we assume that the thickness of the wetting layer d_w is much smaller than d. A slightly more rigorous estimate leads to the curvature $2/(d - 2d_w)$.

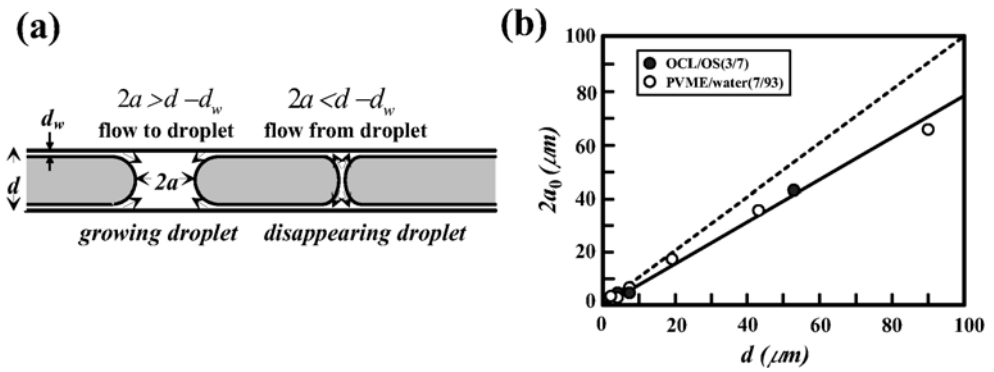

Figure 8. (a) A schematic diagram of growing and disappearing droplets (tubes) in a 2D capillary. (b) The dependence of the threshold radius of a droplet for its growth, $2a_0$, on the spacing d. The dashed line is the line of $2a_0 = d$. The smaller slope compared to this prediction may simply reflect a geometrical factor, e.g. the finite thickness of the wetting layer. $2a_0$ increases linearly with d. Our study indicates that this behaviour is independent of the kind of mixture and universal.

With increasing d, the number of bridges (droplets) that finally remain decreases. This can be explained by the condition $2a > d$ becoming more difficult to satisfy for a larger d, since in a bicontinuous structure the number of percolation paths decreases with increase in d and further bicontinuous tubes are spontaneously broken by any asymmetry during the coarsening. The former simply reflects the fact that the number of tubes decreases with coarsening, while the latter is caused by the asymmetry induced by the formation of wetting layers and also by the slight composition asymmetry. Thus the morphological evolution in this configuration is strongly dependent on the gap d. This reflects the fact that there are two relevant length scales in this problem, namely, the domain size a and the thickness of a liquid film d.

5. Late-stage domain growth in a 2D capillary

5.1. The regime of individual growth of tubes bridging the two wetting layers

Once the diameter $2a$ exceeds the thickness d, it grows linearly with time until the interaction between droplets starts to play a role [34]. This linear growth behaviour can be explained by the hydrodynamic flow from the wetting layer into the 2D disc-like droplet being largely dominated by the pressure gradient coming from the longitudinal curvature $2/(d - 2d_w)$. In this approximation, $\mathrm{d}a/\mathrm{d}t \propto (\sigma/\eta)g(d, d_w)$ where $g(d, d_w)$ is a function of d and the wetting layer thickness d_w. Neglecting the temporal change in d_w, we can predict that a grows linearly with time. This was indeed confirmed experimentally, as shown in figure 9. The slowing down of the droplet growth in the late stage may be caused either by the temporal change in d_w or by the interdroplet interaction through the wetting layer. The importance of the effects of the change in d_w was recently pointed out by Wang and Composto [10]. Since the amount of fluid in the wetting layer between neighbouring droplets is finite, droplets cannot absorb the wetting layer independently in the late stage. In both cases, $g(d, d_w)$ becomes a function of time through the change in d_w in this intermediate stage.

5.2. Interdroplet interaction via wetting layers

In the intermediated stage the droplets strongly attract each other by absorbing the wetting layers and also by the capillary instability of the tube formed between neighbouring droplets

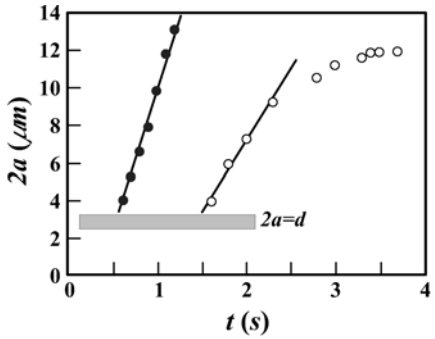

Figure 9. A plot of the droplet radius a bridging the upper and the lower wetting layer against time t for PVME/water (7/93) in a 2D capillary ($d \sim 3$ μm). Open circles: 33.3 °C; filled circles: 34.0 °C. The difference in the slope, which should be proportional to σ/η, reflects the difference in the interface tension σ, which is an increasing function of the quench depth ΔT (note that $\sigma \sim (\Delta T)^{2\nu}$).

[35]. The coarsening behaviour in this stage is shown in figure 10. This interesting behaviour can be explained as follows. The wetting layers connect neighbouring droplets, which are composed of the more wettable phase. Thus the bow-shaped nearest sides of the neighbouring droplets and the upper and lower wetting layers between these droplets form a tube of the less wettable phase. This situation is shown schematically in figure 11. The droplets are attracted to each other to reduce the interface energy of this fluid tube. This phenomenon is essentially the same as the Rayleigh instability in a 1D capillary [33]. The existence of such a tube is confirmed by the fact that the collision of droplets leaves a small droplet inside the droplet after coalescence, as shown in figure 10. This droplet is formed by the capillary instability of a fluid tube between the droplets. Note that the fastest-growing unstable mode has a wavelength of the order of the diameter of the tube, which roughly determines the size of a trapped droplet. The mechanism is shown schematically in figure 12.

The behaviour of droplet collision can be analysed on the basis of a Navier–Stokes equation:

$$\eta[\partial^2 v/\partial y^2 + \partial^2 v/\partial z^2] = \mathrm{d}P/\mathrm{d}x \tag{8}$$

where v is the flow velocity along x, η is the viscosity, and P is the pressure. As indicated in figure 11, x is along the tube axis, z is the thickness direction, and y is perpendicular to x and z. Here we define $\Delta l_{\min}$ as the minimum interdroplet distance (see figure 11). Thus the flow velocity v is related to the interface velocity $\mathrm{d}\,\Delta l_{\min}/\mathrm{d}t$ as $v \sim (L/\Delta l_{\min})\,\mathrm{d}\,\Delta l_{\min}/\mathrm{d}t$, from mass conservation. Reflecting the longitudinal change in the transverse curvature of the tube, the capillary pressure in the tube roughly varies as $\sigma/\Delta l_{\min}$ (σ: interface tension between the two coexisting phases) over the characteristic length along the tube ($\sim L$). Here L can be estimated by the in-plane radius of the local curvature of the fronts of the attracting droplets. Thus, $\mathrm{d}P/\mathrm{d}x \sim \sigma/(\Delta l_{\min} L)$. This pressure gradient causes the Poiseuille flow from the neck to the bulges of the tube. For $\Delta l_{\min} < d$, v is estimated from the relation $\eta v/\Delta l_{\min}^2 \sim \mathrm{d}P/\mathrm{d}x$ (see equation (8)) as

$$v \sim \sigma\,\Delta l_{\min}/(\eta L).$$

Provided that $L = k_\sigma\,\Delta l_{\min}$ (k_σ: constant), we obtain

$$\Delta l_{\min} \sim k_\sigma^{-2}(\sigma/\eta)\,\Delta t. \tag{9}$$

Here Δt is the time to the direct collision. That is, $\Delta t = t_c - t$, where t is the time and t_c is the time of the collision. The linear dependence of L on $\Delta l_{\min}$ assumed above seems to be

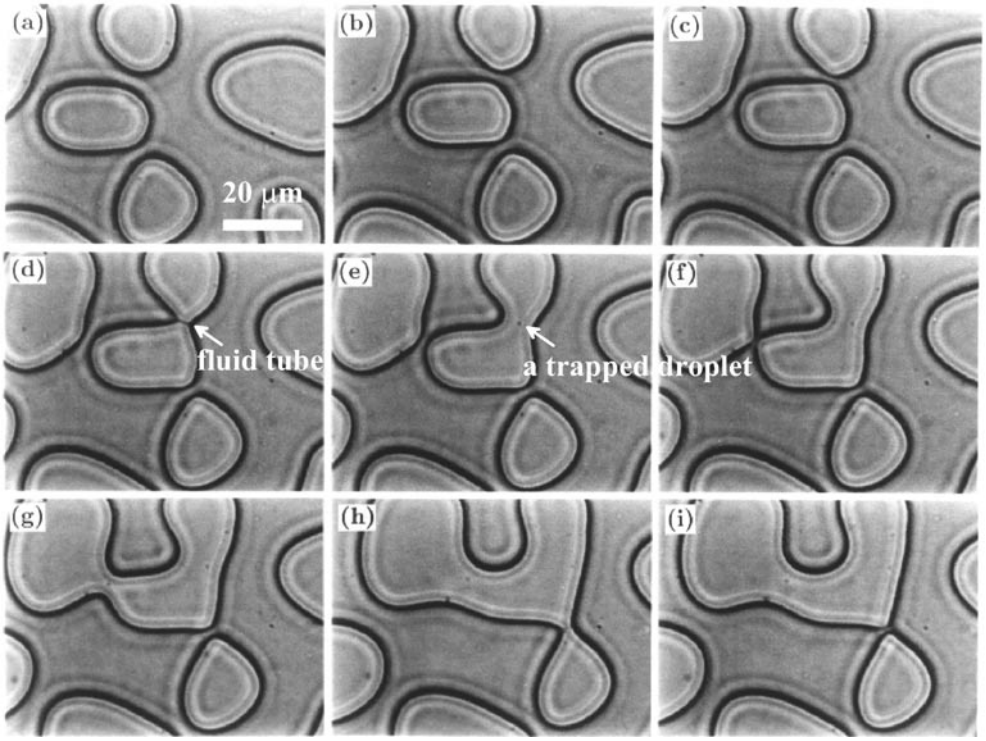

Figure 10. A coarsening process of droplets interacting via wetting layers. The effective attractive interaction between droplets induces frequent interdroplet collisions. The system is PS/PVME (5/5). (a) 855 s, (b) 900 s, (c) 910 s, (d) 920 s, (e) 930 s, (f) 940 s, (g) 950 s, (h) 980 s, and (i) 990 s after the temperature quench.

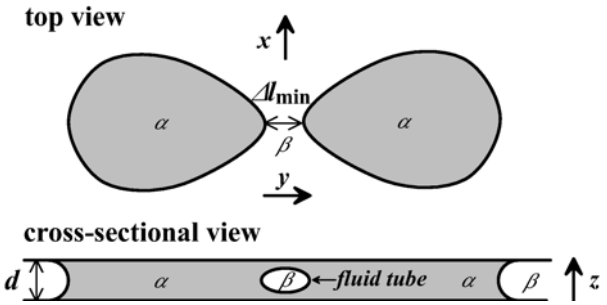

Figure 11. Schematic side and top views of attracting droplets.

reasonable because (i) $\Delta l_{\min}$ is the only relevant length scale of the problem and further (ii) the curvature of the deforming droplet front tends to be balanced by the transverse curvature of the tube ($\sim 1/\Delta l_{\min}$) (see figures 10 and 11). For $\Delta l_{\min} > d$, on the other hand, v is estimated from the relation $\eta v/d^2 \sim \mathrm{d}P/\mathrm{d}x$ (see equation (8)) as

$$v \sim \sigma d^2/(\eta L\, \Delta l_{\min}).$$

Provided again that $L = k_\sigma\, \Delta l_{\min}$, the following relation is obtained:

$$\Delta l_{\min} \sim k_\sigma^{-2}(\sigma d^2/\eta)^{1/3}\, \Delta t^{1/3}. \tag{10}$$

Thus $\Delta l_{\min}$ is predicted to be proportional to Δt for $\Delta l_{\min} < d$ and $\Delta t^{1/3}$ for $\Delta l_{\min} > d$. This prediction is consistent with our experimental results [35], as shown in figure 13. Note that

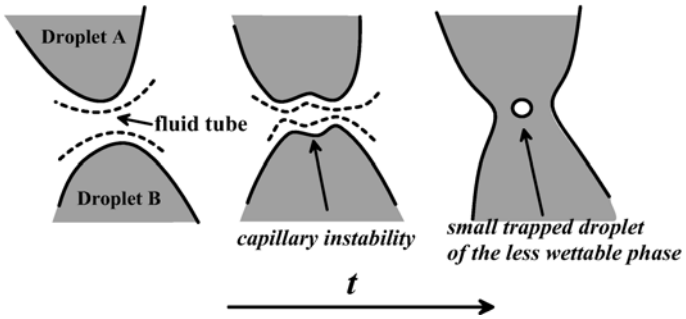

Figure 12. The mechanism of formation of a small droplet from a tube during droplet coalescence.

the crossover from $t^{1/3}$-dependence to t-linear dependence occurs around $\Delta l_{\min} \sim d$; more strictly, $\Delta l_{\min} \sim (d - 2d_w)$, consistently with our prediction. We can also notice that (i) the proportionality constants of relations (9) and (10) both increase with the phase-separation temperature and (ii) they both decrease with increase in the phase-separation time, t_{ps}. The former can be explained by the increase of σ with increasing temperature distance from the critical temperature, ΔT. We speculate that the latter is due to the fact that k_σ is an increasing function of the domain size: a larger domain is more difficult to deform to make a large local curvature of the order of $1/\Delta l_{\min}$ around the colliding point. The relevance of this argument should be checked more carefully in the future. Finally, it should be noted that there is no motion of the centre of mass of the droplets prior to collision, which indicates that this collision process is purely driven by the capillary instability of the tube of the non-wettable phase, and not by translational diffusional motion of droplets.

5.3. Change in the apparent 2D composition symmetry: temporal decrease in the total volume of wetting fluid layers

In a nearly symmetric binary mixture confined in a 2D capillary, the morphology transforms from a 3D interconnected pattern to a 2D droplet pattern and back to a 2D interconnected pattern [35] (see figure 3(c)). This unusual behaviour can be explained from the static aspect as follows: the composition symmetry initially leads to the bicontinuous pattern in bulk. Then the in-plane symmetry of the order parameter is broken by the existence of the wetting layer. This leads to the quasi-2D droplet morphology. Finally, the in-plane symmetry approaches the bulk composition symmetry, since the wetting layers are absorbed into the domains bridging the glass plates. This is supported by the increase in the total droplet area with t_{ps}. Thus the morphology transforms from a droplet pattern to an interconnected pattern again. Such a temporal change in the total droplet area was reported by Bodensohn and Goldburg [32].

Next we discuss the second morphological transition on the basis of the kinetics of the elementary process. During phase separation, the deformation of a droplet shape is generally caused by interdroplet coalescences whose interval is characterized by the collision interval (τ_c). The resulting shape relaxation process is characterized by the relaxation time τ_σ. The wetting effect drastically shortens τ_c compared to that for the usual case without wetting since (1) there is the wetting-induced attractive interaction as already described and (2) the average interdroplet distance becomes smaller with the phase-separation time, reflecting the increase in the in-plane symmetry. Further, the attractive interaction prevents the free shape relaxation and thus τ_σ is increased. The rate of the wetting-induced coarsening is mainly determined by the wetting layer and not strongly correlated with the droplet size. On the other hand, the shape relaxation time is determined by the surface/volume ratio and is proportional to the domain

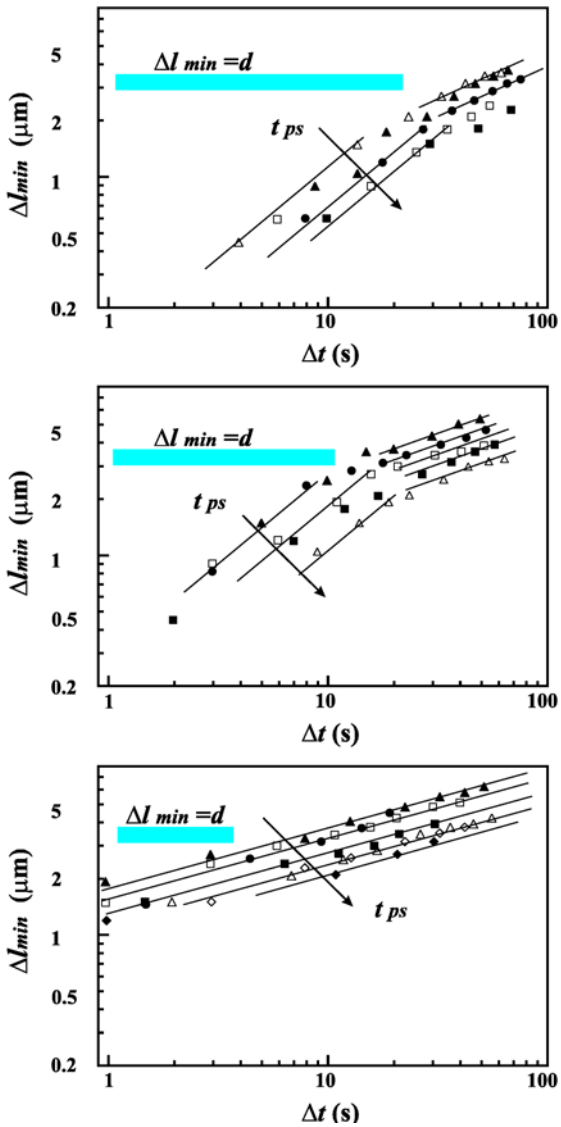

Figure 13. Plots of $\Delta l_{\min}$ against Δt for three phase-separation temperatures. Δt is the time to a direct contact upon collision. Top: 175 °C; middle: 180 °C; bottom: 190 °C. The grey bar indicates the location of $\Delta l_{\min}$ comparable to the gap d. Note that around $\Delta l_{\min} = d$ the transition from $\Delta t^{1/3}$ to Δt-linear dependence of $\Delta l_{\min}$ takes place. t_{ps} is the phase-separation time.

size R. Accordingly, the shape relaxation time increases with the phase-separation time and becomes longer than the collision interval at a certain time. This crossover between the two characteristic times is also responsible for the morphological transformation from an isolated to an interconnected structure.

6. Wetting-induced double phase separation

Next we consider unusual phenomena of double phase separation found in various fluid mixtures.

6.1. Experimental evidence

First we give the experimental evidence for wetting-induced double phase separation [38, 39]. Figure 14 shows the pattern evolution of the PVME/water (7/93) mixture confined in a 1D capillary. Surprisingly, retarded secondary phase separation was observed inside the macroscopically separated phases. This can be noticed around 1 s after the quench from the fact that the two phases look cloudy. Then the droplet pattern becomes visible around 20 s after the quench. This unusual double phase separation (DPS) was not observed for a shallow quench ($\Delta T \leqslant 0.6$ K) (see figure 3 in reference [39]). DPS looks similar to the pattern caused by a temperature double quench [51–53]. The same behaviour of double phase separation was also observed for a 2D capillary in a few binary mixtures, which indicates the general nature of this phenomenon.

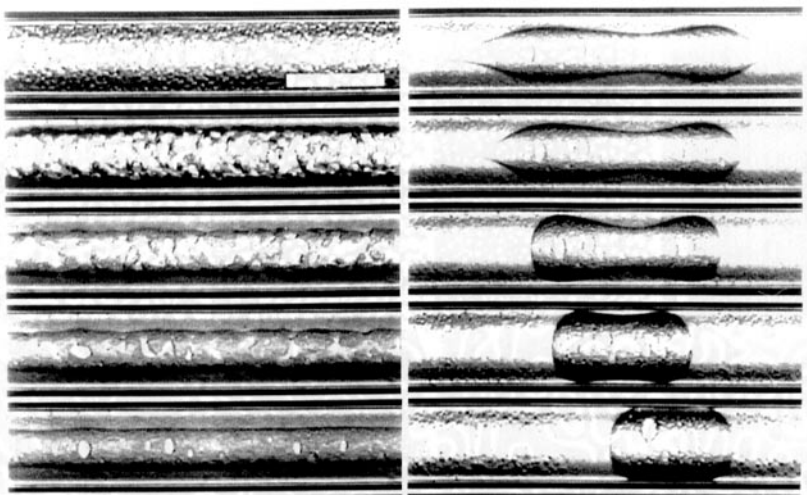

Figure 14. Phase separation in a 1D capillary for PVME/water (7/93). The photographs correspond to 0.3 s, 0.8 s, 1.3 s, 1.8 s, 3.8 s (left column), 22.3 s, 23.8 s, 28.8 s, 88.8 s, and 479 s (right column) from top to bottom, respectively, after the temperature jump from 32.5 °C to 34.0 °C. The bar corresponds to 200 μm. Secondary phase separation can be clearly seen.

We also found that DPS is strongly suppressed by the strong spatial confinement [38, 39]. For a thick sample, DPS was clearly observed, while for a thin sample ($d < 1$ μm), it was not observed even though the other experimental conditions were the same. This fact indicates the importance of bicontinuous phase separation in bulk. It should be noted that for any mixtures, DPS was observed only near the symmetric composition, and even for a deep quench, it was never observed in asymmetric compositions, where droplet phase separation occurs.

All these facts strongly suggest that quick hydrodynamic coarsening accompanied by bicontinuous phase separation plays a crucial role in this phenomenon.

6.2. Possible physical mechanisms of double phase separation

6.2.1. The effect of a finite quench rate. The simplest explanation of the observed phenomena may be that double phase separation is caused by a non-ideality of the temperature quench, namely, a finite quench rate [38, 39], as in the case of a double temperature quench [51–53]. Phase separation starts during the temperature quench process and enters into a rather late stage quickly. A further temperature change makes the two macroscopic phases metastable or

unstable and induces secondary phase separation. However, the following facts seem not to be fully explained by this mechanism. This phenomenon was observed neither for bicontinuous phase separation in a very thin sample nor for droplet phase separation. On noting that the thermal conduction is primarily limited by the glass wall, it is rather difficult to imagine how a slight change in sample thickness can affect the overall quench rate significantly. Note that the thickness of the glass walls is $\sim$150 μm while that of the sample is a few μm. Of course, however, further experimental studies are still necessary to completely rule out this possibility.

6.2.2. The interface quench effect. Here we propose another possible 'physical' mechanism for DPS, which may be conceptually important for the understanding of hydrodynamic effects. In all the mixtures studied, bicontinuous phase separation was observed in the initial stage (see the first photographs in figure 14) because of the composition symmetry. In bicontinuous phase separation, the total interface area of the system is drastically reduced within a short time by the hydrodynamic coarsening originating from the coupling between the concentration and the velocity fields. According to Siggia's mechanism [13], the interface area per unit volume s is estimated to decrease as $s \propto [(\sigma/\eta)t]^{-1}$, where σ is the interface tension and η is the viscosity. Note that in figure 14 the area of the interface between the two phases decreases quite rapidly with time and after only 2 s it has almost disappeared. We call this quick reduction of the interface area 'interface quench'. Since the hydrodynamic interface motion is much faster than the concentration diffusion, *the hydrodynamic flow due to the capillary instability causes only the geometrical coarsening and does not accompany the concentration change.* Thus the system cannot respond to the rapid decrease in the interface energy; that is, the local equilibrium cannot be established. This causes a kind of double-quench effect, which we call *interface quench*. In all the previous studies [1, 2] local equilibrium has been assumed in the hydrodynamic regime, but this may not be correct in the exact sense, especially under surface fields.

Here we mention the difference in coarsening dynamics of a symmetric mixture between phase separation in a confined geometry and bulk phase separation. For both cases the coarsening dynamics is dominated by hydrodynamic tube instability [33]. The difference in the prefactor k in the relation $R = k(\sigma/\eta)t$ may be the only difference [33]. Here $k = k_b$ *or* k_w for bulk and wetting phase separation, respectively. For phase separation under the influence of wetting, k_w is roughly estimated as $\sim$0.1 from Poiseuille's formula. For bulk phase separation, on the other hand, the tube flow is essentially caused by the fluctuations of the interface curvature. San Miguel *et al* [54] theoretically estimated k_b as 0.04 for two-phase fluids having similar viscosity, which was experimentally supported [15]. If we employ $k_b \sim 0.04$, the difference between k_b and k_w is probably within one order of magnitude. However, the anisotropic ordering for wetting phase separation might accelerate the reduction of the interface area further. Thus, we expect the effect of interface quench to be more significant for phase separation under geometrical confinement than for that in bulk.

To check the relevance of the above scenario of DPS, we have to clarify whether the concentration diffusion can follow this quick change in the local equilibrium concentration or not. The time required to hydrodynamically form the macroscopic phase having a domain size R is estimated as $\tau_h \sim R\eta/(k\sigma)$. On the other hand, the characteristic diffusion time for the domain size R is given by $\tau_D \sim R^2/D$, where D is the diffusion constant and $D = k_BT/(5\pi\eta\xi)$ (k_B: Boltzmann's constant). Thus the ratio between τ_h and τ_D is given by $\tau_h/\tau_D = D\eta/(k\sigma R)$. From the two-scale-factor universality, $\sigma = A_\sigma k_BT/\xi^2$, where A_σ is the universal constant in the critical regime and $A_\sigma \sim 0.2$ in 3D [1]. Using this relation and the expression for D, we obtain the relation $\tau_h/\tau_D \sim \xi/(5\pi A_\sigma kR) \sim \xi/(3kR)$. For $\tau_h < \tau_D$, the concentration is different from its equilibrium value and local equilibrium cannot be established. Thus the

interface quench is initiated around $\tau_h/\tau_D \sim 1$. For wetting phase separation ($k_w \sim 0.1$), $R_t \sim 3\xi$ (R_t: the transient domain size when the *interface quench* is initiated). For bulk phase separation ($k_b \sim 0.04$), on the other hand, we obtain $R_t \sim 10\xi$ or $\tau_t \sim 100$ ($\tau_t = t/\tau_\xi$, where $\tau_\xi = \xi^2/D$) from the condition $\tau_h/\tau_D \sim 1$.

All the above estimations are based on the universal behaviour in the critical regime. In the mean-field regime, however, σ/η can be larger than that in the critical regime. Thus, we expect stronger effects of interface quench for the deep temperature quench into the mean-field regime. This consideration leads to an interesting possibility that double phase separation may be induced spontaneously *even in bulk* if we deeply quench a fluid mixture into the mean-field regime.

The validity of this concept of interface quench was checked by numerical simulations of the phase separation of a 2D fluid mixture [55]. For the case of high fluidity, it was demonstrated that the double phase separation is indeed 'spontaneously' induced by the interface quench effect.

The beginning of the *interface quench* characterized by these values of R_t/ξ and τ_t is consistent with the crossover from the slow diffusion growth to the fast hydrodynamic growth in the scaled plots of $2\pi R/\xi$ against t/τ_ξ [38,39]. The *interface quench* may bring the system into a new non-equilibrium (unstable or metastable) state and thus cause the retarded secondary phase separation. The situation is shown schematically in figure 15. Our interpretation of the phenomenon is consistent with the light scattering data given by Wiltzius and Cumming [29], which indicates that (1) the secondary phase separation (in our notation) has the growth law $R \sim t^{1/3}$, unique to the droplet pattern, and (2) it starts to appear just after the hydrodynamic process (the fast mode in their notation [29]) starts to play a dominant role in coarsening (around $\tau_h = \tau_D$) (see figure 13 in reference [43]).

Further studies on the possible effects of interface quench from experimental, theoretical, and numerical viewpoints are highly desirable.

6.3. History-preserving domain growth

Here we briefly mention an interesting example of pattern evolution induced by double phase separation. In contrast to the general phenomenology of liquid–liquid phase separation in which the memory of the structure is continuously lost with time upon coarsening, we found an unusual phase-separation morphology that memorizes the full history of pattern evolution for a binary liquid mixture [56]. The spatial distribution of small solid-like droplets produced by wetting-induced double phase separation records the contact line of colliding droplets. The

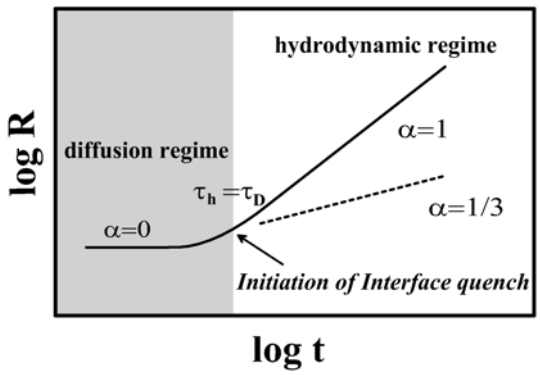

Figure 15. A schematic diagram of the coarsening process of DPS.

solid nature of the droplets is induced by the high glass-transition temperature of a less wettable phase. The collision history preserved in the trajectory pattern of each droplet demonstrates a strong space-time correlation in the structural development during phase separation of nearly symmetric mixtures. An example is shown in figure 16.

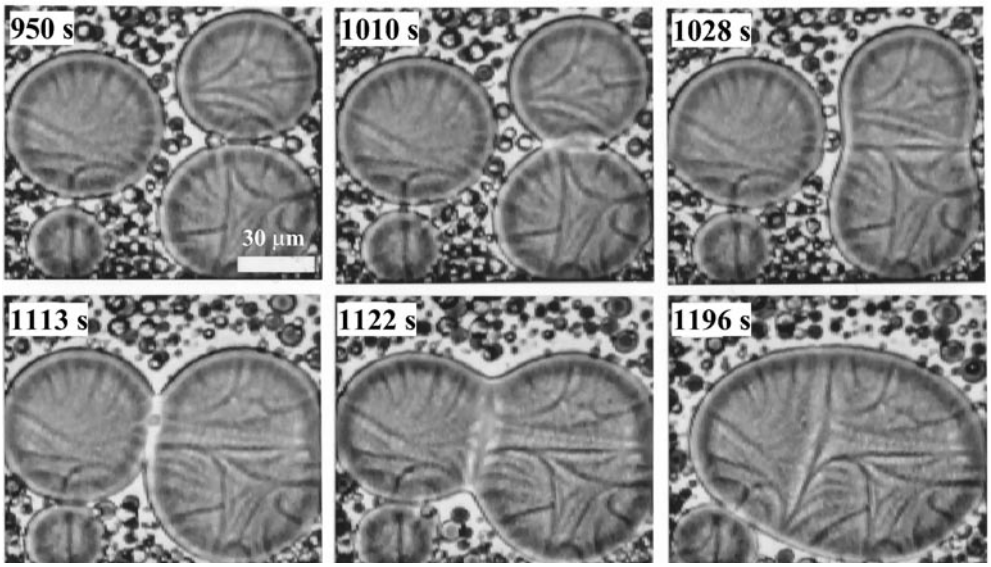

Figure 16. History-preserving droplet phase separation observed in an OCL/OS (3/7) mixture. The temperature was quenched from 140 °C to 60 °C at $t = 0$ s. (a) 950 s, (b) 1010 s, (c) 1028 s, (d) 1113 s, (e) 1122 s, and (f) 1196 s after the temperature quench.

7. Effects of preferential wetting of solid particles

In the above, we discuss the effects of preferential wetting of solid planar or cylindrical substrates on phase separation. It is also interesting to consider the effects of wetting of particles [57]. This problem is of practical importance in the field of composite material, e.g. polymer blends with filler particles [57, 58]. In particular, if solid particles are mobile, their motion can be involved in the pattern-evolution process as a result of the dynamic coupling between wetting and phase separation. Here we consider binary polymer mixtures containing solid spherical particles. As an ideal system, we choose monodisperse glass spheres as the solid particles and study the pattern evolution caused by phase separation. The cooperative effect of phase separation and dynamic wetting leads to an interesting pattern evolution in the system. For numerical studies of this problem, see reference [58] and references therein.

7.1. Geometrical configuration and experimental details

First we have to specify the geometrical configuration which we are going to consider. Although there can be a variety of configurations, we focus here just on the experimental configuration which we employed in our previous experiments [57]. Two grades of monodisperse spherical glass particles were used: GP1 having a diameter of 3.786 ± 0.027 μm, and GP2 with a diameter of 7.088 ± 0.050 μm. The thickness of the sample d was controlled by using GP2 as a spacer. In one series of experiments, we used glass particles of only one type (GP2),

which acted as spacers and also as immobile fillers. These particles cannot move because of the large friction against the glass plates. In the other series of experiments we used a small number of larger-size GP2 spheres as spacers and we also put in a large number of small-size GP1 spheres; in this case, the smaller particles (GP1), which can be regarded as fillers, can move freely inside the quasi-2D sample. We call the former the 'immobile particle case' and the latter the 'mobile particle case'. We believe that the essential features will not be affected by the details of experimental conditions.

7.2. Basic principle: energetic aspect

First we discuss the static energetic aspect of the problem, assuming the above geometrical configuration. The total free energy of the system per unit volume can be given by

$$F = 4\pi a^2[\gamma_\alpha n_\alpha + \gamma_\beta n_\beta] + \frac{1}{d}\left[\gamma_\alpha\left(\Phi_\alpha + \frac{4}{3}\pi R_{GP}^3 n_\alpha\right) + \gamma_\beta\left(\Phi_\beta + \frac{4}{3}\pi R_{GP}^3 n_\beta\right)\right] + \sigma f(d). \tag{11}$$

Here the α- and β-phases are the OCL-rich and OS-rich phases, respectively, and n_α and n_β are the number of the particles per unit volume in the α- and β-phases, respectively. Φ_α and Φ_β are, respectively, the volume fractions of the α- and β-phases normalized by the total volume of the sample including spheres. Thus, $\Phi_\alpha + \Phi_\beta + \Phi_{GP} = 1$, where Φ_{GP} is the volume fraction of glass particles. R_{GP} is the radius of the glass spheres. γ_α and γ_β are the energies of interaction between the glass and the α- and β-phases, respectively. σ is the interfacial tension between the α- and β-phases. $f(d)$ is the total area of the interface between the α- and β-phases per unit volume. The first two terms in the above free energy are related to the wettability of the glass particles, the next two terms to the wettability of the glass plates, and the last term to the interfacial energy between the α- and β-phases. Here it should be noted that the wettability of the glass plates plays little role in the late-stage phase separation after the formation of bridges between the plates. All the interesting effects of glass particles on phase separation originate from the interplay between the first two terms and the last term in the right-hand side of equation (11).

7.3. Effects of particle mobility on pattern evolution

Here we consider the effect of particle mobility on the pattern evolution under the influence of wetting of particles. After the formation of a sharp interface, the wetting layers are quickly formed on the surfaces of both glass spheres and glass plates by the hydrodynamic process unique to nearly symmetric binary mixtures [33–35]. This wetting layer forms an interconnected structure, so the particles are bridged by it. Once the droplets are bridged by the more wettable phase, the strong attractive interaction acts between the droplets to reduce the α–β interface area. This interaction is very long range because of the interconnected nature of the wetting layer. Thus, the phase-separation pattern evolves such that the more wettable phase includes all the particles. When this attractive force is weaker than the particle trapping force, particles cannot move (an immobile particle case), and vice versa (a mobile particle case). Below we consider the pattern evolution for both immobile and mobile particle cases.

7.3.1. Wetting of immobile particles. In this case, the more wettable OCL-rich phase forms domains around the glass particles to reduce the solid–liquid interfacial energy, as shown in figure 17. Since the glass spheres are hard to move, only those glass particles that are close

enough can be bridged by the OCL-rich phase. The coarsening process completely stops in this rather early stage, because domains are pinned by the fixed glass particles.

For the case of immobile particles, the final structure is determined by the competition between $\Delta\gamma$ $(=\gamma_\beta - \gamma_\alpha)$ and σ. That is, inclusion of the particle into the α-phase, which is driven by $\Delta\gamma$, competes with the formation of large domains, which is driven by σ. This leads to the final pattern composed of small domains, where most of the particles are included in the α-phase, even though there remains a rather large area of interface between the α- and β-phases. The final size of the domain is determined by the number density of particles, their spatial distribution, and the composition symmetry of the mixture. In addition to the energetic argument, consideration of the dynamics also leads to the conclusion that coarsening stops at a finite size. Coarsening of the droplet pattern is usually dominated by the evaporation–condensation and/or Brownian-coagulation mechanisms [1, 13]. In our case, however, neither

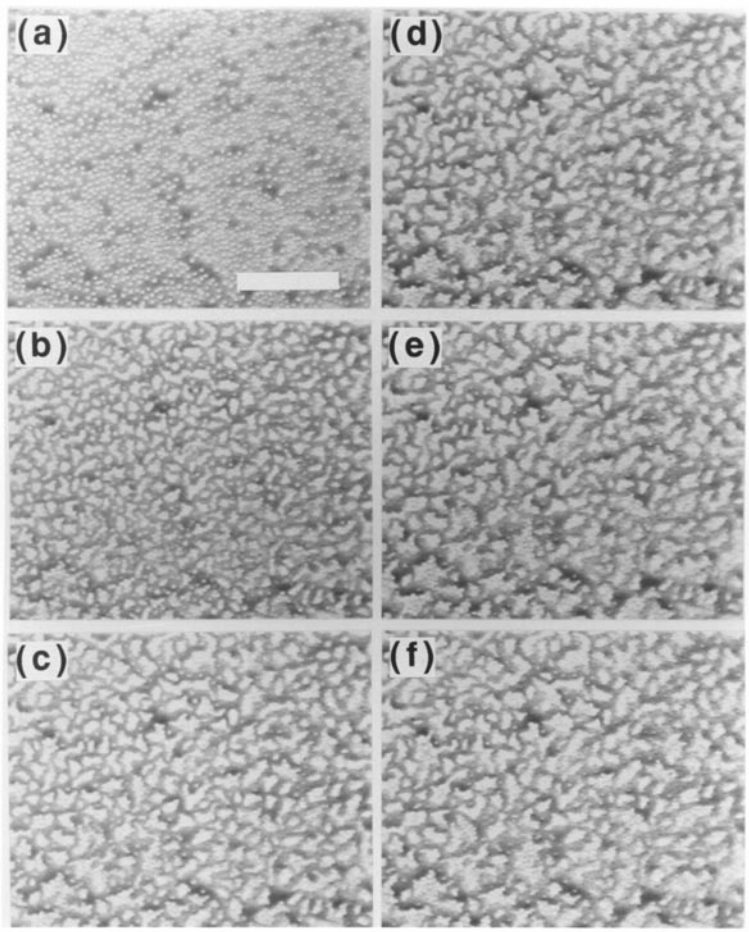

Figure 17. Phase separation in OCL/OS (3/7) with immobile glass beads. $d = 7.1$ μm. The temperature was quenched from 140 °C to 100 °C. (a) 16 s, (b) 60 s, (c) 120 s, (d) 300 s, (e) 600 s, and (f) 1200 s. The bar corresponds to 100 μm. The number density ρ_n of the GP1 spheres is $\sim 1.2 \times 10^6$ cm^{-2}: their volume loading fraction Φ_{GP} is ∼9% and their projected-area loading fraction S_{GP} is ∼14%.

of these mechanisms can act efficiently. Droplet motion is prevented by the pinning effect of the fixed glass spheres (*a strong spatial pinning effect*) and thus the Brownian-coagulation mechanism does not work after the formation of a metastable domain structure. For a domain to move, it has to dewet the particles included in it. The motion of a droplet, which requires the dewetting of N particles, has to overcome an energy barrier of $4\pi R_{GP}^2 N \Delta\gamma$. This large energy barrier is strong enough to prevent the thermal motion of the droplet. Further, the local curvature of a domain is not correlated with the domain size and it is determined by the spatial distribution of the glass particles; thus the evaporation–condensation mechanism does not work either. These considerations lead to the conclusion that after all glass particles are bridged by the more wettable α-phase droplets, the droplet pattern is stabilized for both static and kinetic reasons. Thus, the coarsening, even if it occurs, is extremely slow. We need further studies to answer on a quantitative level the question of what determines the characteristic length of the final domain structures.

7.3.2. Wetting of mobile particles. Next we consider the case of mobile particles. The system also tries to reduce the free energy by lowering the energetic factors relating to $\Delta\gamma$ and σ. The former leads to inclusion of the glass particles into the α-phase domains, while the latter causes coarsening of the domains. Although this feature is the same as in the case of immobile particles, the mobility of particles allows domains to continuously coarsen to reduce the α–β interfacial energy. The pattern evolution can then be classified into the following three cases: (1) $\Phi_\alpha \gg \Phi_{GP}$, (2) $\Phi_\alpha \sim \Phi_{GP}$, and (3) $\Phi_\alpha \ll \Phi_{GP}(1/\phi_{\mathrm{pack}} - 1)$ (ϕ_{pack}: the closest-packing volume fraction).

For case (1), the inclusion of the particles occurs first, and then the domains gradually grow by the wetting-layer-induced attractive interaction mechanism as well as by the Brownian-coagulation and evaporation–condensation mechanisms. Figure 18 corresponds to such a case. In contrast to the case of immobile particles, all the glass particles are completely included inside the α-phase droplet, or the droplet attains a spherical shape, because of their mobility. Thus the curvature is directly determined by the droplet size. However, the coarsening rate is slow compared to that in the case without particles, where domains coarsen as $a \sim t^{1/3}$ (a: the characteristic domain size) [20, 21]. Glass particles may reduce the translational motion of a droplet since the local velocity difference between the fluid inside the droplet and the spheres probably causes additional friction opposing the droplet motion (*a weak spatial pinning effect of particles*). However, it is not clear how significantly this effect slows down coarsening, and thus further studies are highly desirable.

For case (2), the packing density of the glass particles inside the α-phase becomes very high and the glass particles locally form an ordered structure because of their geometrical confinement, which is a result of minimization of the $\Delta\gamma$ interaction. The ordered structure prevents the domains from deforming and coarsening further since there is a high potential barrier to deforming the ordered hexagonal packing of the glass spheres. This spontaneous pinning effect due to particle ordering (*a shape pinning effect of ordered particles*) slows down the coarsening of domains (see figure 19). In the enlarged view shown in figure 20, we can clearly see the ordered structures of particles confined in the more wettable domains. Between cases (1) and (2), the coarsening rate becomes maximal ($a \sim t^{1/3}$) [57] because the increase of Φ_{GP} has two competing factors:

(i) The increase of Φ_{GP} induces the transformation of the phase-separation pattern from a droplet one to a bicontinuous one. This accelerates the domain coarsening since a bicontinuous pattern makes quick hydrodynamic coarsening possible.
(ii) On the other hand, the further increase of Φ_{GP} induces shape pinning effects as a result

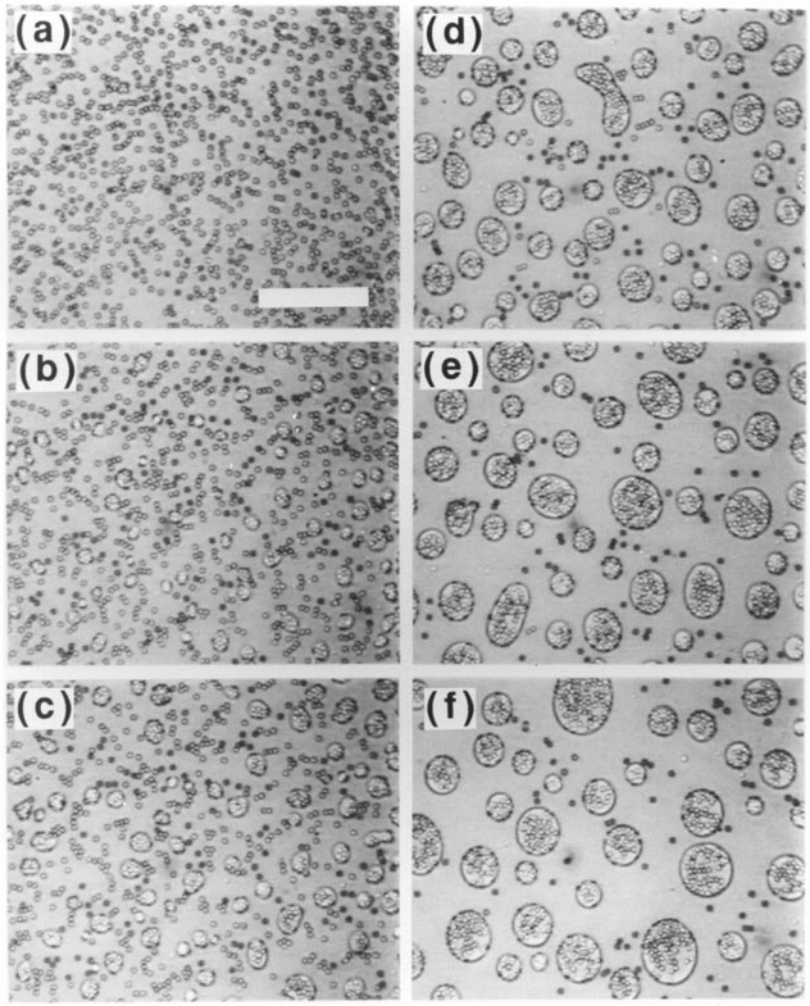

Figure 18. Phase separation in OCL/OS (3/7) with mobile glass beads. $\Phi_{GP} \sim 3.2\%$ and $S_{GP} \sim 9\%$. $d = 7.1$ μm. The temperature was quenched from 140 °C to 60 °C. (a) 0 s, (b) 10 s, (c) 30 s, (d) 150 s, (e) 390 s, and (f) 1710 s. The bar corresponds to 100 μm.

of the ordering of particles confined in the domain.

The competition of these two opposite effects naturally explains why the coarsening rate has a maximum as a function of Φ_{GP}.

For a high particle concentration (see figure 21), the interface of the domain becomes rather rough (not smooth) and the shape relaxation of the domain due to interface tension becomes ineffective due to the effects of strong confinement on particles and the resulting close packing. The coarsening becomes very slow for this case.

For case (3), there may be coexistence of closely packed glass particles that are included in the α-phase with particles that cannot be included in it. This is simply because there is no way for all particles to be included in the α-phase. Cases (1) and (2) and case (3) may be named 'complete wetting' and 'partial wetting', respectively, although the physical origin of the appearance of the two states is essentially different from that for a planar substrate. This

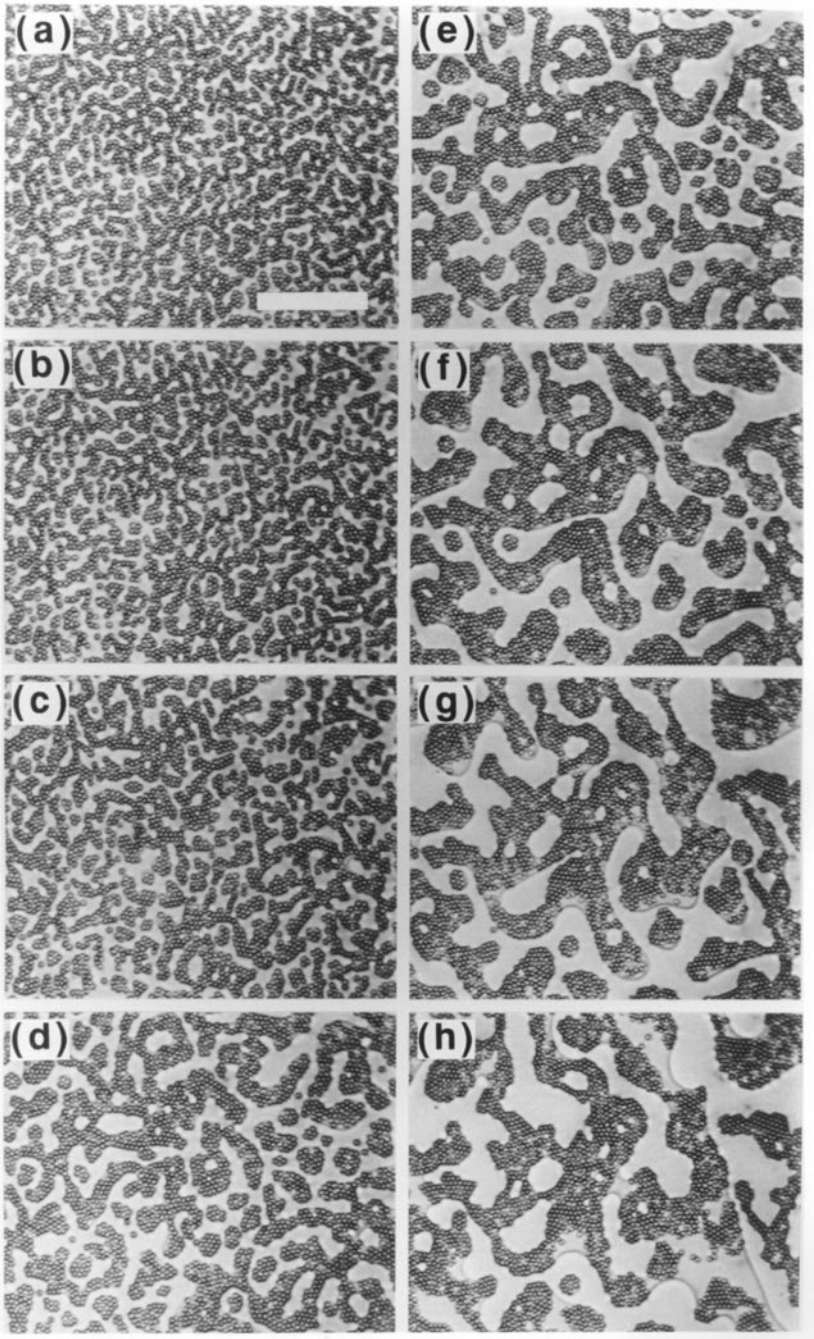

Figure 19. Phase separation in OCL/OS (3/7) with mobile glass beads. $d = 7.1\ \mu$m. $\Phi_{GP} \sim 5.2\%$ and $S_{GP} \sim 15\%$. The temperature was quenched from 140 °C to 60 °C. (a) 6 s, (b) 10 s, (c) 20 s, (d) 60 s, (e) 120 s, (f) 300 s, (g) 600 s, and (h) 1660 s. The bar corresponds to 100 μm.

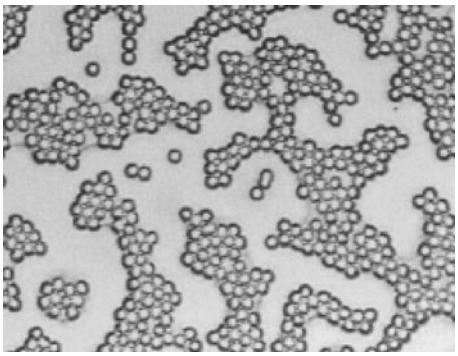

Figure 20. Phase separation in OCL/OS (3/7) with mobile glass beads observed with a higher magnification. The condition is the same as that for figure 19. Here we can see individual glass particles clearly.

may be an example of a geometrically induced complete–partial wetting transition.

Since most of the glass particles are included in the α-phase except in the case where $\Phi_{GP} \gg \Phi_\alpha$, the apparent volume fraction of the α-phase becomes $\Phi_\alpha + \Phi_{GP}$. Thus the bicontinuous structure appears when $\Phi_\alpha + \Phi_{GP} \sim 1/2$. The morphology can be changed by controlling Φ_{GP}, even for a fixed ratio between the α- and β-phases. Such behaviour is actually observed in figures 18–21.

7.4. Potential applications

From an applications viewpoint, this study strongly indicates that it is possible to intentionally control the final domain size in phase separation by means of the spatial arrangement of a fixed solid phase, and also to control the final morphology by inducing the spontaneous pinning effect with addition of a certain amount of mobile solid particles. These ideas may be applied to the physical design of composite materials including polymer alloys and polymer-dispersed liquid-crystal displays. By changing the volume fraction of particles, we can control the apparent symmetry of the composition—namely, whether the final pattern becomes bicontinuous or isolated. The selective inclusion of solid particles into the more wettable phase and the resulting particle ordering may be universal to all binary liquid mixtures including solid particles, irrespective of experimental conditions such as particle shape, particle size, their distribution, and film thickness. So far the structures of these mixtures have been considered mainly from the static energetic standpoint, but our study indicates the importance of the dynamic aspect.

Finally, we consider some interesting physical problems associated with this spontaneous inclusion of particles into the more wettable phase. In the above we consider the case of spherical particles without long-range interactions. In this case, the spatial confinement may induce the crystallization or vitrification of particles. If the charged colloidal particles are confined in an aqueous droplet, we may realize the soft crystallization of these particles. The same idea can be applied to rods and plates. Liquid-crystal ordering to nematic and smectic phases is expected for such cases. Furthermore, the following problem is also quite interesting. What happens when we mix two types of particle, one of which favours the A component while the other favours the B component, into a mixture of A and B, and let the mixture phase-separate? For a dilute particle concentration, we expect the perfect partitioning of particles into the two phases. This may open up a new way of achieving particle separation. For a higher particle concentration, the situation is much more complicated due to the slow dynamics induced by the high packing density due to strong confinement, which prevents the wetting-induced spontaneous partitioning of particles. This kind of problem should be studied in the near future.

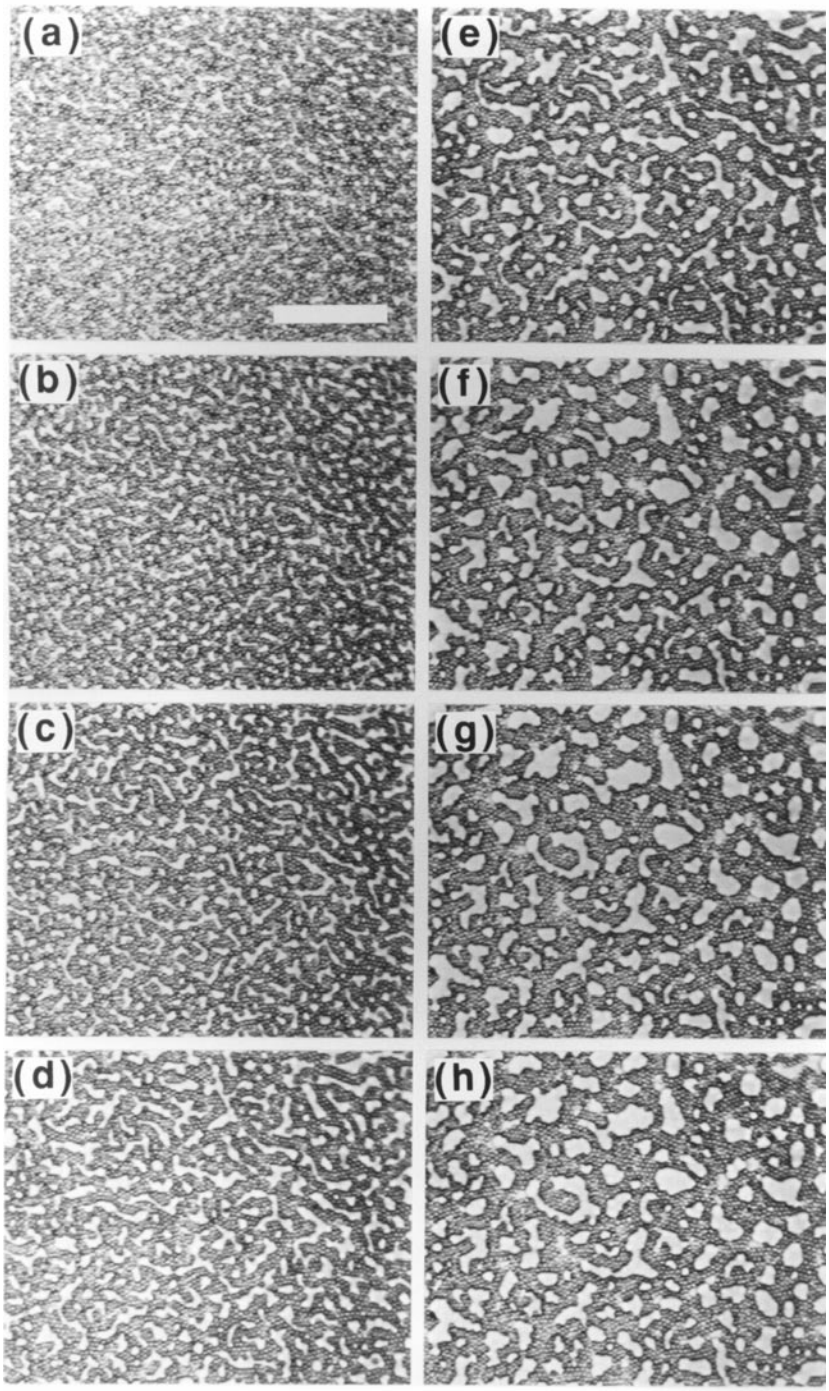

Figure 21. Phase separation in OCL/OS (3/7) with mobile glass beads. $d = 7.1\ \mu$m. $\Phi_{GP} \sim 19\%$ and $S_{GP} \sim 53\%$. The temperature was quenched from 140 °C to 60 °C. (a) 16 s, (b) 20 s, (c) 30 s, (d) 50 s, (e) 120 s, (f) 600 s, (g) 2100 s, and (h) 3180 s. The bar corresponds to 100 μm.

8. Numerical simulations

Numerical simulation is one of the most powerful ways to study phase separation under the influence of surface fields (see references [7, 8] and references therein). The formation of the composition wave in surface-directed spinodal decomposition has been particularly well studied. Here we check the validity of the mechanisms proposed above by using three-dimensional (3D) numerical simulations of fluid phase separation under the influence of surface fields. Although there are some interesting studies on two-dimensional (2D) fluid phase separation under wetting effects [41,47], from the case of bulk phase separation the behaviour in 3D [13] is expected to even be qualitatively different from that in 2D [54]. Hereafter we explain the results of our numerical simulations [50], focusing on the roles of hydrodynamics. Below, we do not consider the effects of wetting of particles on phase separation. For such simulation studies, see reference [58] and references therein.

8.1. Simulation methods

Here we limit our interest to a symmetric [50:50] mixture of A and B. The solid surface that favours A more than B is introduced at $z = 0$ by means of $f_s(\phi)$ with $a = b = -1$ (see equation (7)), which corresponds to a 'complete wetting' condition [3]. Here positive ϕ means A-rich phase. The scaled versions of equations (1), (2), and (7) are solved by the Euler method under the incompressibility condition $\boldsymbol{\nabla} \cdot \boldsymbol{V} = 0$ with the boundary conditions $V_z = 0$ and $\partial\mu/\partial z = 0$ at $z = 0$ and with periodic boundary conditions along the x- and y-directions. The system size was $64 \times 64 \times 64$ for 3D.

We choose the grid size $\Delta x = \Delta y = \Delta z = 1$ and the time step $\Delta t = 0.01$ to ensure numerical stability. We do not use the steady-state approximation ($\partial \boldsymbol{V}/\partial t = 0$) to handle the non-periodic boundary condition imposed by the wall. Instead, the velocity fields are calculated in real space by solving

$$\partial \boldsymbol{V}/\partial t = \Gamma \boldsymbol{F} - \boldsymbol{\nabla} P + \Xi \nabla^2 \boldsymbol{V}.$$

We calculate $\Gamma \boldsymbol{F} - \boldsymbol{\nabla} P$ by means of an inverse Fourier transformation of $\boldsymbol{D}_q \cdot \Gamma \boldsymbol{F}_q$, where $\boldsymbol{D}_q = \boldsymbol{I} - \boldsymbol{qq}/q^2$. (Note that $\boldsymbol{\nabla} \cdot (\Gamma \boldsymbol{F} - \boldsymbol{\nabla} P) = 0$ since $\boldsymbol{\nabla} \cdot \boldsymbol{V} = 0$.) Random noises of ϕ (10^{-3} in amplitude) are introduced only at $t = 0$, while velocity noises are not introduced at all.

8.2. Evolution of the pattern and flow fields

Figure 22 shows the overall pattern evolution during spinodal decomposition under the surface fields of a wall set at the bottom ($z = 0$). In this figure, we display an interface of $\phi = 0$. It should be noted that for $t \leqslant 40$ a sharp interface has not yet formed, although the figure gives us the impression of the existence of a sharp interface. The apparent multi-layer structure near the interface is not real, but just reflects the composition wave. Initially, the composition wave, or the composition oscillation along the z-direction, is observed near the wall, as is well known [6–8, 26, 28, 37, 45, 46, 48]. Then, there occur sequentially the destruction of the composition wave, the formation of a wetting layer of the A-rich phase, and its thickening. We can clearly see that bicontinuous tubes are connected directly to the wetting layer.

In section 4 we proposed that the hydrodynamic pumping of the more wettable phase into the wetting layer induces the thickening of the wetting layer. The existence of such a directional flow into the wetting layer is confirmed by figure 23, which shows the flow fields along the z-direction in a horizontal view. It should be noted that this flow spreads on the wetting layer, which causes the radial thickening of a part of a fluid tube connected to the wetting layer. This leads to the faster coarsening near the wetting layer, as will be discussed in section 8.5. All

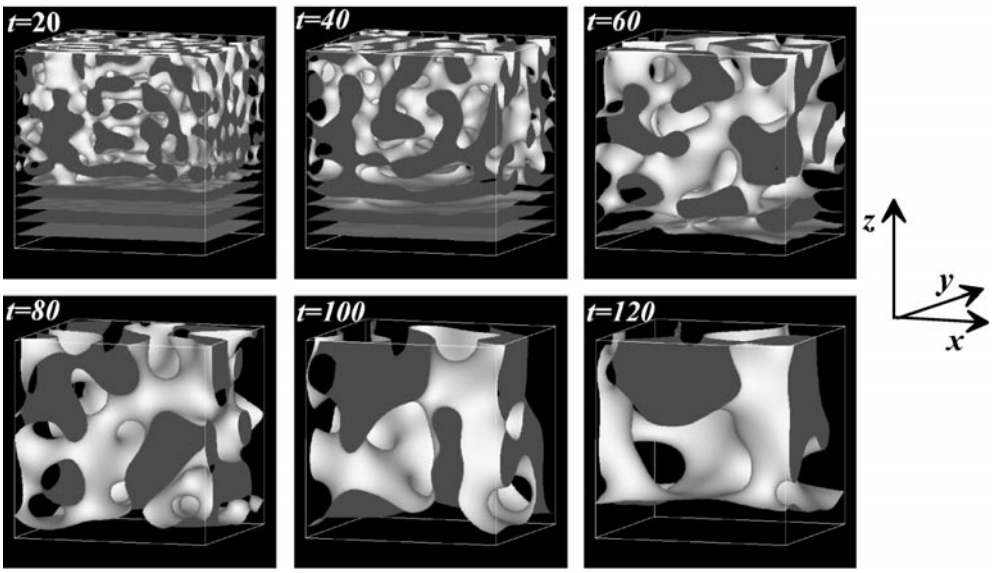

Figure 22. 3D pattern evolution during spinodal decomposition under the influence of wetting of the solid wall at the bottom ($z = 0$). Here $\Gamma = 10$ and $\Xi = 1$.

these effects are due to the pressure in fluid tubes of a bulk bicontinuous structure being higher than that in a wetting layer by $\sim\sigma/a_{\rm tube}$ ($a_{\rm tube}$: the radius of the fluid tubes) [33, 34, 37].

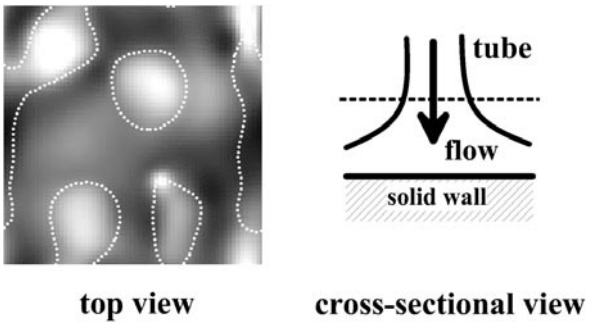

Figure 23. Left: flow fields at $t = 80$ near the wall in an x–y plane ($z = 12$) parallel to the wall. The white dotted curves indicate the domain or tube interface. The contrast of the greyscale image represents V_z: white means flow toward the wall, while black means flow in the opposite direction. Here $\Gamma = 10$ and $\Xi = 1$. Right: a schematic diagram showing a cross-sectional view in the x–z plane.

8.3. Transition from a diffusion to a hydrodynamic regime

Here we discuss (i) the formation of a composition wave, (ii) its disappearance, and (iii) the thickening dynamics of a wetting layer. As can be seen clearly in figure 22, a composition wave is first formed near the surface. This process is dominated by the diffusion process. Note that hydrodynamic effects are very weak since the sharp interface has not formed at this stage. The appearance of the composition wave near the surface is a direct consequence

of the symmetry-breaking surface fields. Its physical mechanism has already been discussed intensively [6–8, 26, 28, 37, 45, 46, 48]. Thus, we do not repeat the discussion here.

Later on, the composition wave is gradually destroyed by the growing bulk composition fluctuations that are basically isotropic. Since hydrodynamic effects produce the material flow toward the wall, this destruction dynamics of the composition wave is significantly accelerated for a fluid system compared to a solid system [50]. As the composition difference between the two phases $\Delta\phi$ increases and the interface becomes sharper with time, the average velocity of the hydrodynamic flow increases, following the relation $|\boldsymbol{v}| = v \sim (\Delta\phi)^2$ [55]. The hydrodynamic flow from the bulk to the higher-order layers destabilizes the layer structures. Accordingly, the higher-order layers are sequentially destroyed one by one from $t \sim 30$, and eventually a single 'wetting layer' is formed around $t \sim 70$ (see figure 22). Then the hydrodynamic transport of the more wettable phase via fluid tubes becomes a dominant process of the thickening of the wetting layer and the thickness starts to increase linearly with time by a 'hydrodynamic pumping' mechanism [33, 34, 37–39]. It should be noted that bicontinuous fluid tubes are always connected directly and perpendicularly to the surface wetting layer in the late stage (see figure 22). In other words, there is local orientational order in the tube direction near the wall. This destruction of a composition wave and the resulting formation of a single wetting layer are required for the switching of the thickening mechanism of a wetting layer from a diffusional to a hydrodynamic one.

8.4. Thickening kinetics of a wetting layer

The next step is the hydrodynamic thickening of the wetting layer. Figure 24 shows the temporal change in the wetting layer thickness $d_w(t)$ for both solid and fluid mixtures for $\Xi = 1$. For solid mixtures the wetting layer grows as $d_w \sim t^{1/3}$ after the initial transient rapid growth of a wetting layer, which depends on surface parameters (a, b), while for fluid mixtures it initially follows the behaviour of solid mixtures, but later grows as $d_w = k(t - t_c)$. Here t_c is the onset time of hydrodynamic effects, at which $|\boldsymbol{v}|$ in bulk reaches its stationary value of $|\boldsymbol{v}| \sim \sigma/\eta$ [13]. In accord with this, k was found to be proportional to Γ/Ξ ($\propto\sigma/\eta$). This late-stage linear growth is quite consistent with the experimental observation [34, 59] and the theoretical prediction ($d_w \sim (\sigma/\eta)t$) [34, 37–39]. The value of k is estimated to be $\sim$0.1, assuming that the fluidity parameter $R_f = \Gamma/\Xi$ is about 10 in the critical regime. This is also consistent with our previous rough estimation. This confirms the validity of our previous scaling argument. The deviation from the t-linear law for $d_w > 15$ may be due to the finite-size effects.

8.5. Fast lateral coarsening of wetting domains near the wetting layer

Here we demonstrate that the coarsening in a lateral direction is faster near the wetting layer than in the bulk, which might be related to the unusually fast coarsening discussed in section 4.1 [29]. In figure 25, we can clearly see that the domain coarsening near the wetting layer is faster than that in bulk. The coarsening in bulk is well described by $\langle q \rangle \sim t^{-1}$ for $t \geqslant t_c$ (=45), which is typical of 3D spinodal decomposition of fluid mixtures. Note that hydrodynamic transport exceeds diffusional transport for $t \geqslant t_c$ (see figure 26). On the other hand, the fast domain coarsening near the wall can be approximated by $\langle q \rangle \sim t^{-3/2}$. This faster coarsening near the surface is suggestive of the physical origin of the fast-mode kinetics ($\langle q \rangle \sim t^{-3/2}$) observed by Wiltzius and Cumming [29]; that is, the hydrodynamic pumping mechanism should be responsible for the fast-mode kinetics [38, 39].

The onset of this fast coarsening near the surface ($t \sim 100$) coincides well with the time at which the wetting layer starts to thicken because of hydrodynamic effects (see figure 24). Thus,

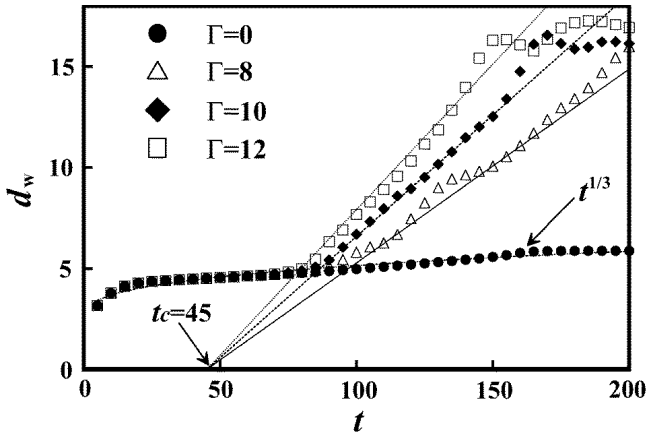

Figure 24. Temporal change in the thickness l of a wetting layer for a solid model ($\Gamma = 0$) and a fluid model ($\Gamma \neq 0$). Here $\Xi = 1$. The curves are $d_w = 2.43{+}0.587t^{1/3}$ and $d_w = 0.0120(\Gamma/\Xi)(t - t_c)$.

this may be regarded as the process of 'hydrodynamic coating' or 'hydrodynamic spreading' of the more wettable phase. This result seems to be consistent with our scenario, which was explained in section 4.1. However, the power-law regime is too short for a conclusive argument and the question of whether it is transient or really asymptotic also remains as a future problem. It is also not clear whether this can naturally explain the observed structure factor or not. Thus, further studies are still required for the unambiguous determination of the physical origin of this fast-growth mode.

8.6. Evidence of the interface quench effect

Here we check the validity of a scenario for double phase separation in which the hydrodynamic thickening of the wetting layer is too quick for a diffusion process to follow and this retardation of diffusion brings the system out of equilibrium [38,39]. To see this effect, we plot in figure 26 the diffusion flux $|\nabla\mu|$ in bulk and that in the wetting layer, together with the hydrodynamic

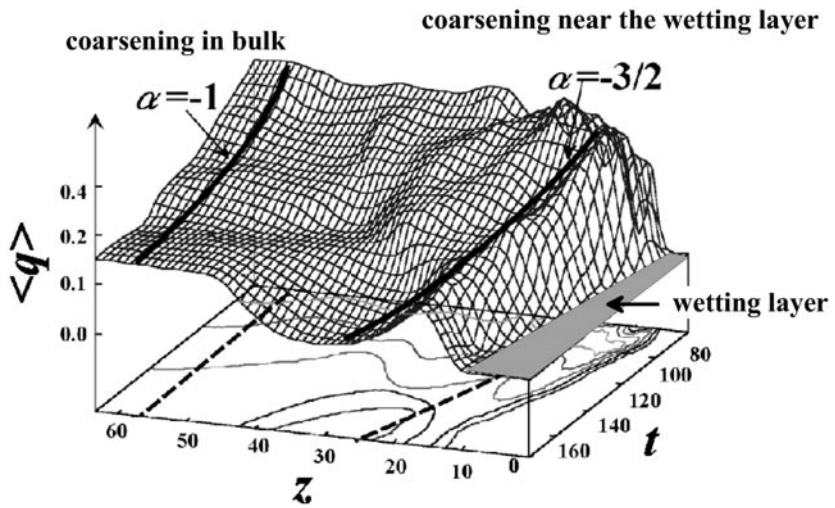

Figure 25. Time development of $\langle q(z)\rangle$. The lateral coarsening near the wall is considerably faster than that in bulk. Here $\Gamma = 10$ and $\Xi = 1$.

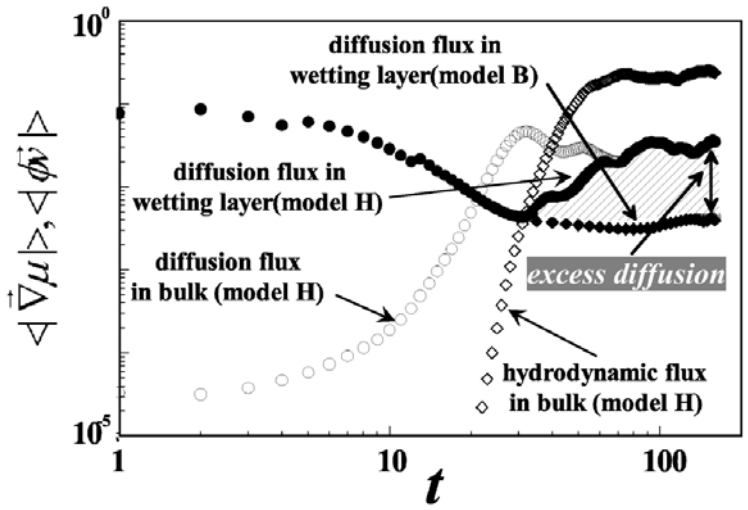

Figure 26. Temporal change in the diffusion flux in the wetting layer and in the bulk together with the growth of the hydrodynamic flux in the bulk. Here $\Gamma = 10$ and $\Xi = 1$. After $t = 30$, there is excess diffusion in the wetting layer for a fluid mixture, which indicates that the diffusion process cannot follow the quick hydrodynamic coarsening process.

flux $|\phi v|$. For a solid mixture, $|\nabla\mu|$ in the wetting layer monotonically decreases with time, while for a fluid mixture it initially decreases with time, but starts to increase around $t \sim 30$. At this time, the hydrodynamic flow from the bulk to the higher-order layers is initiated, as described before, and it also affects the primary wetting layer because of its long-range nature. Since diffusion cannot follow this quick hydrodynamic process, the wetting layer starts to become an out-of-equilibrium one, which enhances the diffusion flux in the wetting layer for $t > 70$. The absence of such effects in a solid system (model B [11]), which is confirmed by our simulation (see figure 26), clearly indicates that this is not due to the surface-potential effects, but due to the hydrodynamic effects. This retardation of the diffusion from rapid hydrodynamic coarsening may even make the phase-separated phases metastable or unstable again and lead to a phenomenon of drastic 'double phase separation' [38, 39, 55], as discussed before.

In different simulations in two dimensions without surface effects, we confirm that the quick hydrodynamic coarsening does indeed cause spontaneous double phase separation for a case of high fluidity. Although the fluidity is a universal, uncontrollable parameter in the critical regime in 3D, it may become large in the mean-field regime. This suggests the possibility of double phase separation even in bulk for a very deep quench. The fluidity can also effectively become large under the surface effects. Further studies are necessary to understand the phenomenon of double phase separation.

9. Summary

In summary, we have discussed the universal features of wetting dynamics unique to a phase-separating binary fluid mixture interacting with solid surfaces, focusing on the roles of hydrodynamics. It was demonstrated that the wetting layer formation in bicontinuous phase separation is strongly dependent on the spatial dimensionality of the geometrical constraint. The hydrodynamic coarsening unique to bicontinuous phase separation delocalizes the wetting

effects and drastically accelerates the wetting dynamics. Thus the macroscopic wetting structure is formed within a short time. A possible mechanism for the fast-mode kinetics was also suggested, although we need further studies for a conclusive argument.

Further, we discussed *double phase separation* (DPS), which was found in confined symmetric binary mixtures. This phenomenon may be universal to all confined symmetric binary mixtures. We demonstrated that this unusual phenomenon may be caused by the *interface quench* effect unique to bicontinuous phase separation. We also suggested a possibility that DPS might be observed even for bulk phase separation under deep quench conditions, where the mean-field picture holds and the fluidity is no longer a universal constant. Effects of preferential wetting of mobile and immobile particles by one component of a phase-separating fluid mixture were also discussed.

The problem of the solid–fluid interaction and its effects on self-organization of a fluid mixture is quite important not only from the fundamental viewpoint, but also from the applications viewpoint. In this article, we do not discuss the wetting effects on a thin film with a free surface [9, 10], the wetting on a patterned surface, and the interplay between wetting and viscoelastic phase separation [60], which are quite important in technological applications. We stress that the basic understanding of the phenomena is necessary for the design of composite material, including material with nanoscale heterostructures and structured biomaterial. In this article, we consider the pattern evolution on a rather macroscopic scale. Pattern formation on a mesoscopic scale will be extremely interesting and important. Even on that length scale, we expect hydrodynamics to play important roles as long as the relevant length scale is comparable to or larger than the correlation length of a fluid mixture. We believe that the basic mechanism described in this article may also be applicable even for these complex problems. At the same time, however, we need a basic understanding of nanorheology, which is important especially for complex fluids with mesoscopic internal length scales.

Acknowledgments

The author is grateful to T Araki, T Koyama, A J Lovinger, and D D Davis for their collaboration in the work reviewed in this article. This work was partly supported by a Grant-in-Aid from the Ministry of Education, Science, Culture, and Sports, Japan.

References

[1] Gunton J D, San Miguel M and Sahni P 1983 *Phase Transitions and Critical Phenomena* vol 8, ed C Domb and J L Lebowitz (London: Academic)
[2] Bray A J 1994 *Adv. Phys.* **43** 357
[3] Cahn J W 1977 *J. Chem. Phys.* **66** 3667
[4] Jasnow D 1984 *Rep. Prog. Phys.* **47** 1059
[5] de Gennes P G 1985 *Rev. Mod. Phys.* **57** 827
[6] Krausch G 1995 *Mater. Sci. Eng. Rep.* R **14** 1
[7] Puri S and Frisch H L 1997 *J. Phys.: Condens. Matter* **9** 2109
[8] Binder K 1998 *J. Non-Equil. Thermodyn.* **23** 1
[9] Karim A, Slawecki T M, Kumar S K, Douglas J F, Satija S K, Han C C, Russell T P, Liu Y, Overney R, Sokolov O and Rafailovich M H 1998 *Macromolecules* **31** 857
[10] Wang H and Composto R J 2000 *J. Chem. Phys.* **113** 10 386
[11] Hohenberg P C and Halperin B I 1976 *Rev. Mod. Phys.* **49** 435
[12] Kawasaki K and Ohta T 1983 *Physica* A **118** 175
[13] Siggia E D 1979 *Phys. Rev.* A **20** 1979
[14] Chou Y C and Goldburg W I 1979 *Phys. Rev.* A **20** 2105
[15] Wong N C and Knobler C M 1981 *Phys. Rev.* A **24** 3205

[16] Guenoun P, Gastaud R, Perrot F and Beysens D 1987 *Phys. Rev.* A **36** 4876
[17] Hashimoto T, Itakura M and Shimazu N 1986 *J. Chem. Phys.* **85** 6118
[18] Bates F S and Wiltzius P 1989 *J. Chem. Phys.* **91** 3258
[19] Ohta T 1984 *Ann. Phys., NY* **158** 31
[20] Tanaka H 1994 *Phys. Rev. Lett.* **72** 1702
Tanaka H 1995 *J. Chem. Phys.* **103** 2361
[21] Tanaka H 1996 *J. Chem. Phys.* **105** 10 099
[22] Tanaka H 1997 *J. Chem. Phys.* **107** 3734
[23] Kumaran V 1998 *J. Chem. Phys.* **109** 7644
Kumaran V 2000 *J. Chem. Phys.* **112** 10 984
[24] Liu A J, Durian D J, Herbolzheimer E and Safran S A 1990 *Phys. Rev. Lett.* **65** 1897
[25] Williams K and Dawe R A 1987 *J. Colloid Interface Sci.* **117** 81
[26] Ball R C and Essery R L H 1990 *J. Phys.: Condens. Matter* **2** 10 303
[27] Guenoun P, Beysens D and Robert M 1990 *Phys. Rev. Lett.* **65** 2406
[28] Jones R A L, Norton L J, Kramer E J, Bates F S and Wiltzius P 1991 *Phys. Rev. Lett* **66** 1326
[29] Wiltzius P and Cumming A 1991 *Phys. Rev. Lett.* **66** 3000
[30] Bruder F and Brenn R 1992 *Phys. Rev. Lett.* **69** 624
[31] Steiner U, Klein J, Eiser E, Budkowski A and Fetter L J 1992 *Science* **258** 1126
Steiner U and Klein J 1996 *Phys. Rev. Lett.* **77** 2546
[32] Bodensohn J and Goldburg W I 1992 *Phys. Rev.* A **46** 5084
[33] Tanaka H 1993 *Phys. Rev. Lett.* **70** 53
[34] Tanaka H 1993 *Phys. Rev. Lett.* **70** 2770
[35] Tanaka H 1993 *Europhys. Lett.* **24** 665
[36] Tanaka H and Koyama T, unpublished
[37] Marko J F 1993 *Phys. Rev.* E **48** 2861
[38] Tanaka H 1994 *Phys. Rev. Lett.* **72** 3690
[39] Tanaka H 1995 *Phys. Rev.* E **51** 1313
[40] Troian S M 1993 *Phys. Rev. Lett.* **71** 1399
Troian S M 1994 *Phys. Rev. Lett.* **72** 3739
[41] Keblinski P, Ma W J, Maritan A, Koplik J and Banavar J 1993 *Phys. Rev.* E **47** R2265
Keblinski P, Ma W J, Maritan A, Koplik J and Banavar J 1994 *Phys. Rev. Lett.* **72** 3738
[42] Tanaka H 1996 *Phys. Rev.* E **54** 1709
[43] Cumming A, Wiltzius P, Bates F S and Rosedale J H 1992 *Phys. Rev.* A **45** 885
[44] Cumming A, Wiltzius P, Bates F S and Rosedale J H 1992 *Phys. Rev.* A **45** 885
Shi B Q, Harrison C and Cumming A 1993 *Phys. Rev. Lett.* **70** 206
Harrison C, Rippard W and Cumming A 1995 *Phys. Rev.* E **52** 723
[45] Puri S and Binder K 1992 *Z. Phys.* B **86** 263
Puri S and Binder K 1992 *Phys. Rev.* A **46** R4487
Puri S and Binder K 1994 *Phys. Rev.* E **49** 5359
[46] Brown G and Chakrabarti A 1992 *Phys. Rev.* A **46** 4829
Brown G, Chakrabarti A and Marko J F 1994 *Phys. Rev.* E **50** 1674
[47] Chen H and Chakrabarti A 1997 *Phys. Rev.* E **55** 5680
[48] Krausch G, Dai C, Kramer E J and Bates F S 1993 *Phys. Rev. Lett.* **71** 3669
Krausch G, Dai C A, Kramer E J, Marko J F and Bates F S 1993 *Macromolecules* **26** 5566
Krausch G, Kramer E J, Bates F S, Marko J F, Brown G and Chakrabarti A 1994 *Macromolecules* **27** 6768
[49] Geoghegan M, Jones R A L, Sivia D S, Penfold J and Clough A S 1996 *Phys. Rev.* E **53** 825
[50] Tanaka H and Araki T 2000 *Europhys. Lett.* **51** 154
[51] Tanaka H 1993 *Phys. Rev.* E **47** 2946
[52] Kwak K D, Okada M, Chiba T and Nose T 1993 *Macromolecules* **26** 4047
[53] Hashimoto T, Hayashi M and Jinnai H 2000 *J. Chem. Phys.* **112** 6886
Hayashi M, Jinnai H and Hashimoto T 2000 *J. Chem. Phys.* **112** 6897
[54] San Miguel M, Grant M and Gunton J D 1985 *Phys. Rev.* A **31** 1001
[55] Tanaka H and Araki T 1998 *Phys. Rev. Lett.* **81** 389
[56] Tanaka H, Lovinger A J and Davis D D 1996 *Phys. Rev.* E **54** R2216
[57] Tanaka H, Lovinger A J and Davis D D 1994 *Phys. Rev. Lett.* **72** 2581
[58] Balazs A C 1999 *Curr. Opin. Colloid Indust.* **4** 443 and see also references therein
[59] Pak H K and Law B M 1995 *Europhys. Lett.* **31** 19
[60] Tanaka H 2000 *J. Phys.: Condens. Matter* **12** R207